

# We are IntechOpen, the world's leading publisher of Open Access books Built by scientists, for scientists

6,900

Open access books available

186,000

International authors and editors

200M

Downloads

Our authors are among the

154

Countries delivered to

TOP 1%

most cited scientists

12.2%

Contributors from top 500 universities



WEB OF SCIENCE™

Selection of our books indexed in the Book Citation Index  
in Web of Science™ Core Collection (BKCI)

Interested in publishing with us?  
Contact [book.department@intechopen.com](mailto:book.department@intechopen.com)

Numbers displayed above are based on latest data collected.  
For more information visit [www.intechopen.com](http://www.intechopen.com)



---

# Investigation of Martensitic Transformation Induced by Cyclic Plastic Deformation in Austenitic Steels

---

Jerzy Kaleta, Przemysław Wiewiórski and  
Wojciech Wiśniewski

Additional information is available at the end of the chapter

<http://dx.doi.org/10.5772/intechopen.71408>

---

## Abstract

The main goal was to demonstrate the possibility of investigating martensitic transformation induced by plastic strain, especially including the kinetics of this transformation, using selected cross effects. It is commonly known that this type of transformation is a basic “mechanism” occurring in shape memory materials and metastable austenitic steels strengthened with martensite separations. The motivation behind the research was also to follow and visualise the transformation on line, during cyclic loading (fatigue process), without the necessity to use, for example, roentgenographic (destructive) or microscopic methods. The application of the magneto-mechanical effect (the Villari effect) and the thermomechanical effect (the Kelvin/Thomson effect) turned out to be particularly useful because they significantly change with martensite initiation and then accumulate in austenite. Therefore, the goal was to develop the non-destructive methods of investigating martensite transformation, which could then be used on real constructions made of metastable austenite steel. In the case of the magneto-mechanical method, the goal was to additionally visualise the magnetic field transformations along a sample in the function of a loading cycle and the index of this period. To achieve this, high-resolution phase maps were used, which also allowed image processing methods known from machinery visioning (MV) or digital image correlation (DIC) techniques to be used.

**Keywords:** martensite transformation induced by plastic strain, transformation kinetics, martensite initiation and accumulation, research methods, cross effects, Villari effect, Kelvin effect

---

# 1. Introduction and purpose of research

## 1.1. Significance of the research problem

**Austenitic steels**, due to their special mechanical, magnetic and technological properties, as well as corrosion resistance, are a material commonly used in the medical, automotive, aircraft, food, chemical, petrochemical and mining industries. The past 100 years of austenite steels have seen many examples of spectacular applications that justify today's position of this class of materials in economy and science. The issue has been widely discussed in numerous publications.

**Martensite transformation** that takes place in austenite steels significantly changes the properties of the input material. The appearance of martensite separations in the austenite matrix results in both positive consequences (e.g. strengthening of material) and negative ones. In other cases, such a change of structure is undesirable (e.g. a decrease in corrosion resistance, lower fatigue and fracture strength, the appearance of an undesirable magnetic phase).

There are two main types of martensite transformation: thermal transformation resulting from austenite supercooling at high speed and also strain-induced transformation resulting from the occurrence of critical plastic deformation. Martensite can also be obtained by the application of a strong magnetic field.

The martensite transformation induced by plastic deformation, including cyclical deformation, is a fundamental "mechanism" occurring in shape memory materials and metastable austenite steels strengthened with martensite separations.

The paper only focuses on the **martensite transformation induced by plastic strain** in metastable austenite steels, induced by cyclic plastic strain, and especially the methodology of investigating the phase transformation. It was considered especially important to develop efficient research methodology on the **kinetics of martensite transformation induced by cyclical plastic strain** using non-destructive methods. This is essential because, for example, the creation of constitutive and fatigue models for this class of materials [1–3] requires the estimation of the quantitative share of martensite as a function of the number of loading cycles.

On the other hand, investigating the kinetics is not easy because in each mechanical loading cycle there is a martensite growth, which means that the material which is initially a single-phase one (austenite) becomes a two-phase material (austenite + martensite). Additionally, the austenite-martensite quantitative ration is systematically changed. It should also be emphasised that the research results encompassing mechanical values (stress, strain, the area of the hysteresis loop, etc.) only allow the behaviour of a two-phase material to be cyclically analysed, without a possibility to obtain more precise information about martensite.

There are a few methods of investigating martensite transformation, amongst others, roentgen diffraction [4–6], neutron diffraction [7], microscopic measurements [6, 8], density [4], hardness measurements [4] as well as magnetic measurements [4–6, 8–12]. There is still a need, however, for non-destructive methods, which would be useful in both laboratory and industrial conditions. This is why, as is stated below, new methods using selected physical cross effects can turn out to be especially effective.

**Transformation in two- and three-dimensional objects.** It is assumed that the martensite transformation induced by plastic strain (which is also the consequence of supercooling) occurs differently in massive objects in which all three dimensions are of the same order (the so-called 3D objects) and also in two-phase objects such as foils (2D objects). In 3D objects, the transformation process is initiated and developed in a different way in the external layer, known as the skin, compared to deeper layers belonging to the so-called core. The other material, that is, 2D, can be treated as the skin, which is a more uniform object.

## 1.2. Research objective

The main goal of the research was to indicate the possibility of investigating the martensite transformation induced by plastic strain using selected cross effects, including mainly the kinetics of this transformation. The application of the magneto-mechanical and thermomechanical effects was considered particularly useful, because, as it was shown, they change significantly with the initiation and later accumulation of martensite in austenite. Hence, the goal was the development of non-destructive research methods of martensite transformation, which could be used both in laboratory conditions and on real constructions made of metastable austenite steel.

Key issues:

- Selection of cross effects and proving their usefulness in the online research on martensite transformation
- Construction of dedicated measurement apparatus for laboratory research which could also be used in industrial conditions
- Verification of the method in laboratory conditions

## 2. Cross effects used to investigate the phase transformation

In the research on the kinetics of martensite transformation induced by plastic strain presented below, the use of two cross effects, namely, the Villari effect and the Kelvin (Thomson) effect, was proposed.

**Villari effect application.** The phenomenon of inverse magnetostriction, also called the Villari effect, is particularly useful in the research on transformation. The essence of the effect was described in numerous earlier publications, also written by the authors of this article [13, 14]. It utilises the susceptibility of the effect of the occurrence of the ferromagnetic phase, that is, martensite  $\alpha'$ . Thus, it is possible to easily detect the moment of transformation initiation after exceeding the cyclical border of plasticity in metastable austenite. It is also possible to assess the martensite phase growth, depending on the level of loading and the number of cycles. The local character of the measurement (due to the small size of a sensor, e.g. a magnetoresistor) allows a particular way of scanning the investigated surface for the purpose of finding a ferromagnetic phase in the "background" of the dominant austenite phase to be conducted.

It was assumed that it would be possible to indirectly investigate the growth of martensite in austenite by analysing the waveform of a selected magnetic component and by “calibrating” it in a certain way. The magnetic signal, which is a representative for martensite separation and accumulation, will be indicated at a later stage.

**Kelvin effect application.** An example of another effective research method is the application of the thermo-elastic phenomenon, also called the Thomson effect or the Kelvin effect. The effect used the fact that in adiabatic conditions—in terms of elastic strains—metals behave like gas. This means that during tension they are cooled down and during compression they are heated up. In a triaxial stress state, the change of temperature  $\Delta T$  is also directly proportional to the sum of changes in the normal stresses ( $\Delta\sigma_{xx}$ ,  $\Delta\sigma_{yy}$ ,  $\Delta\sigma_{zz}$ ) of the linear coefficient of thermal expansion  $\alpha$  and absolute body temperature  $T_0$  and indirectly proportional to density  $\rho$  and the specific heat  $c$  of a body; hence,

$$\Delta T = -\frac{T_0 \cdot \alpha}{\rho \cdot c} (\Delta\sigma_{xx} + \Delta\sigma_{yy} + \Delta\sigma_{zz}) = -k \sum_i \Delta\sigma_i \quad (1)$$

For over 150 years (from 1853) [15], it was thought that this law was well documented experimentally. However, not so long ago, it was found that there was an interesting deviation from the Kelvin model in the case of ferromagnetic materials [16]. **Figure 1**, showing waveforms  $\sigma(\xi)$  and  $\Delta T(\xi)$  [17], presents clear evidence to this.

Sinusoidal stress waveforms—according to Kelvin’s law—should correspond within counter-phase sinusoidal signals of temperature growth  $\Delta T$ . This fact actually occurs until a certain value of loading is reached, before which there is only a paramagnet, that is, austenite. The appearance of even a small amount of martensite  $\alpha'$  (ferromagnetic phase) results in the occurrence of a certain kind of saddle in waveform  $\Delta T(\xi)$  or, in other words, higher harmonic components.

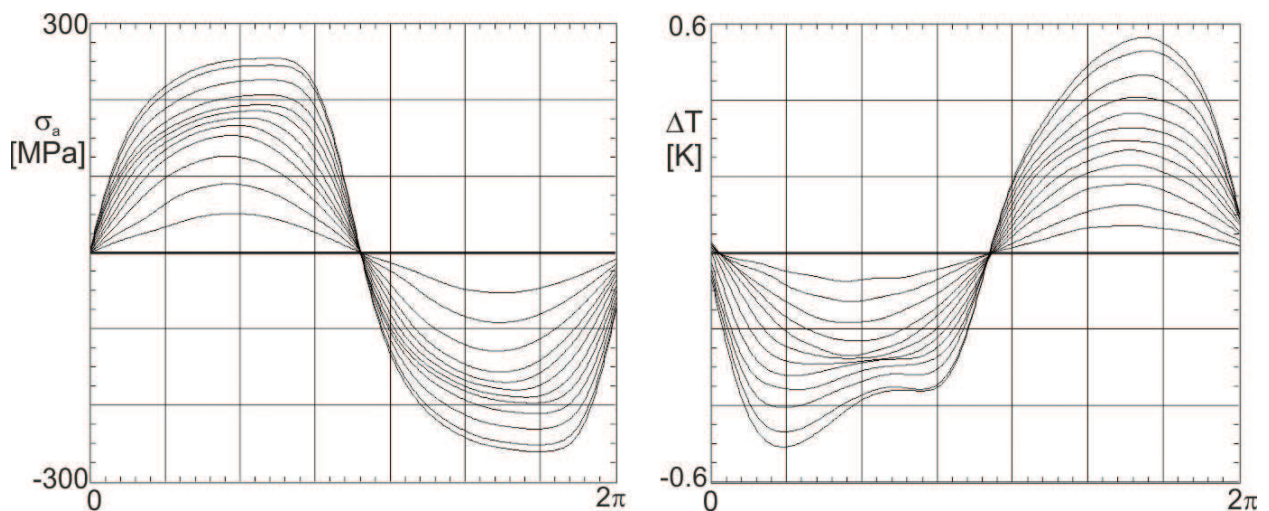


**Figure 1.** Stress waveforms and the temperature growth  $\Delta T$  waveforms corresponding with them, which offer evidence for the occurrence of the martensite transformation induced by plastic strain [17].

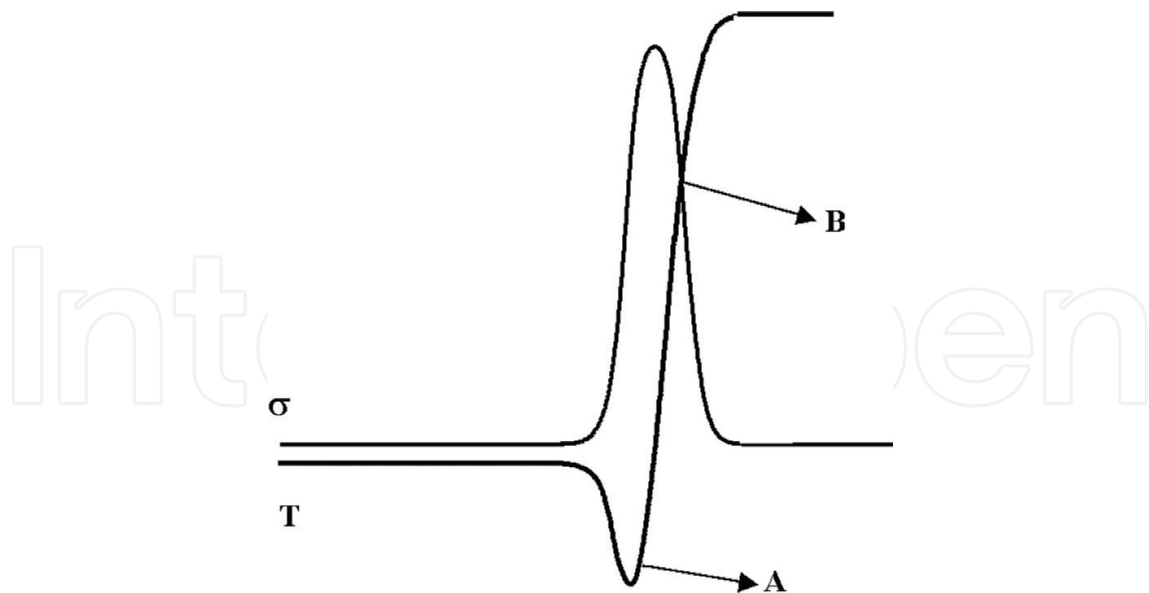


Figure 2. Thomson's law: range of action.

This phenomenon was discovered [16] when temperature was measured with very thin thermocouples (OMEGA type J 0.001" ~ 25  $\mu\text{m}$ ), which have low thermal inertia and allowed higher harmonic components to be registered.

It should be emphasised that the similarity in the behaviour of metals and gases ceases to exist when plastic strain occurs in metal, which is presented in **Figure 2**. It can be observed (**Figure 2**) that temperature decreases with an increase in stress. The appearance of plastic strains in a material is followed by a considerable increase in temperature (point A). At point B, the material returns to the range of plastic strains, and a decrease in load is accompanied by a further growth in temperature because of the occurrence of compression. However, it follows Thomson's law. The temperature change between points A and B confirms the appearance of plastic strains in the material, and the rapid nature of this change is significant enough to be easily observed.

### 3. Evaluation of martensitic transformation induced by plastic deformation in massive specimens

#### 3.1. Research object and measurement setup

The object of the research was to investigate cylindrical samples made of AISI 304 austenite steel. A sample is presented in **Figure 3**, and the chemical composition and strength properties are given in **Table 1**. Before the tests the material was heat treated, and the samples were held at a temperature of 1050°C for 35 minutes and were then quickly cooled in water. The goal of the thermal treatment was to obtain a single-phase material with austenite structure.

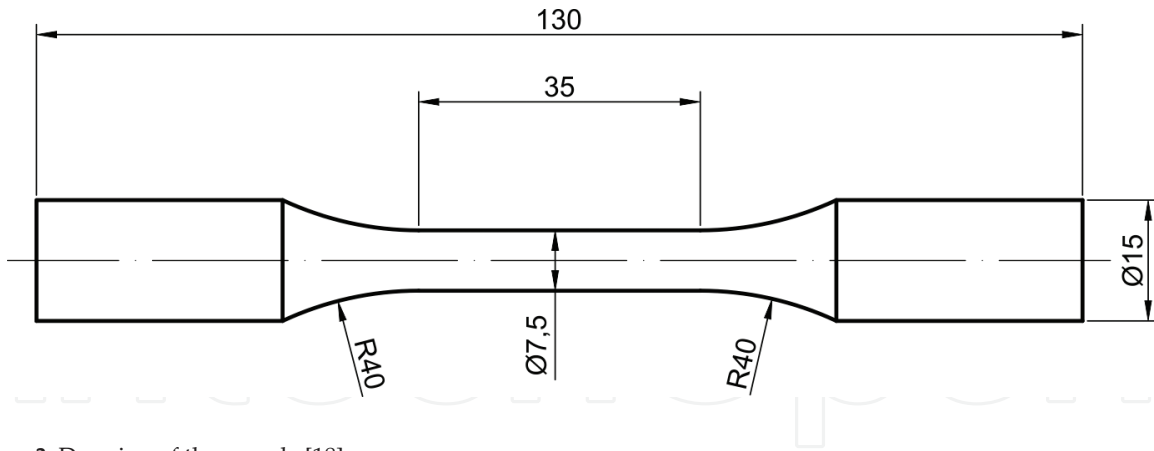


Figure 3. Drawing of the sample [18].

| Material | Chemical composition |       |       |       |       |        |       |       | Strength properties |                |                |
|----------|----------------------|-------|-------|-------|-------|--------|-------|-------|---------------------|----------------|----------------|
|          | C                    | Si    | Mn    | P     | S     | Cr     | Ni    | Ti    | R <sub>e</sub>      | R <sub>m</sub> | A <sub>5</sub> |
|          | %                    | %     | %     | %     | %     | %      | %     | %     | MPa                 | MPa            | %              |
| AISI 304 | 0.018                | 0.297 | 1.402 | 0.032 | 0.026 | 18.347 | 8.757 | 0.006 | 593                 | 752            | 34             |

Table 1. Chemical composition and strength properties of AISI 304 steel [18].

The measurement system was composed of a testing machine MTS 810, computer, extensometer and a magnetic field measuring device (Figure 4). The testing machine was controlled by a FlexTest GT controller and MultiPurpose TestWare Software, which allowed mechanical signals (stress  $\sigma(t)$  and strain  $\epsilon(t)$ ) and magnetic signals (magnetic field strength  $H(t)$ ) to be registered. Magnetic field strength was measured using an original system constructed by the authors' team. In the system, four magnetoresistors KMZ 10B made by Philips (NXT) were used as sensors, and they were arranged in a line according to the sample measurement

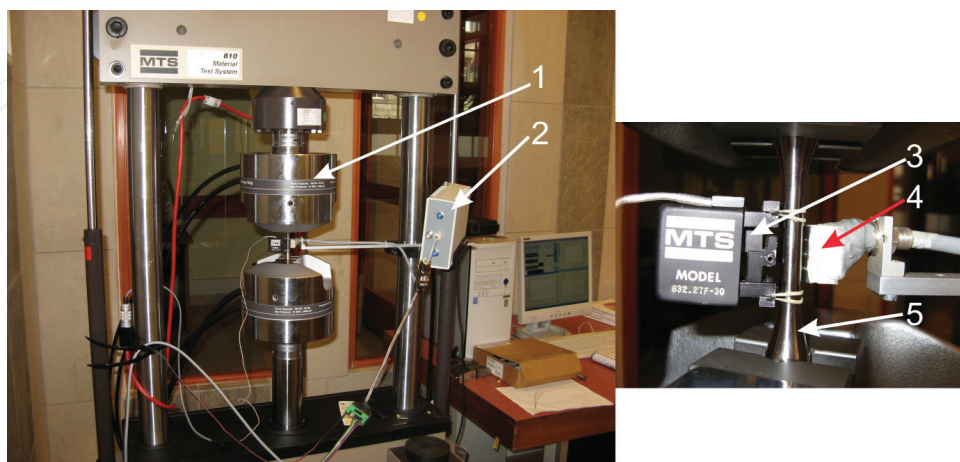
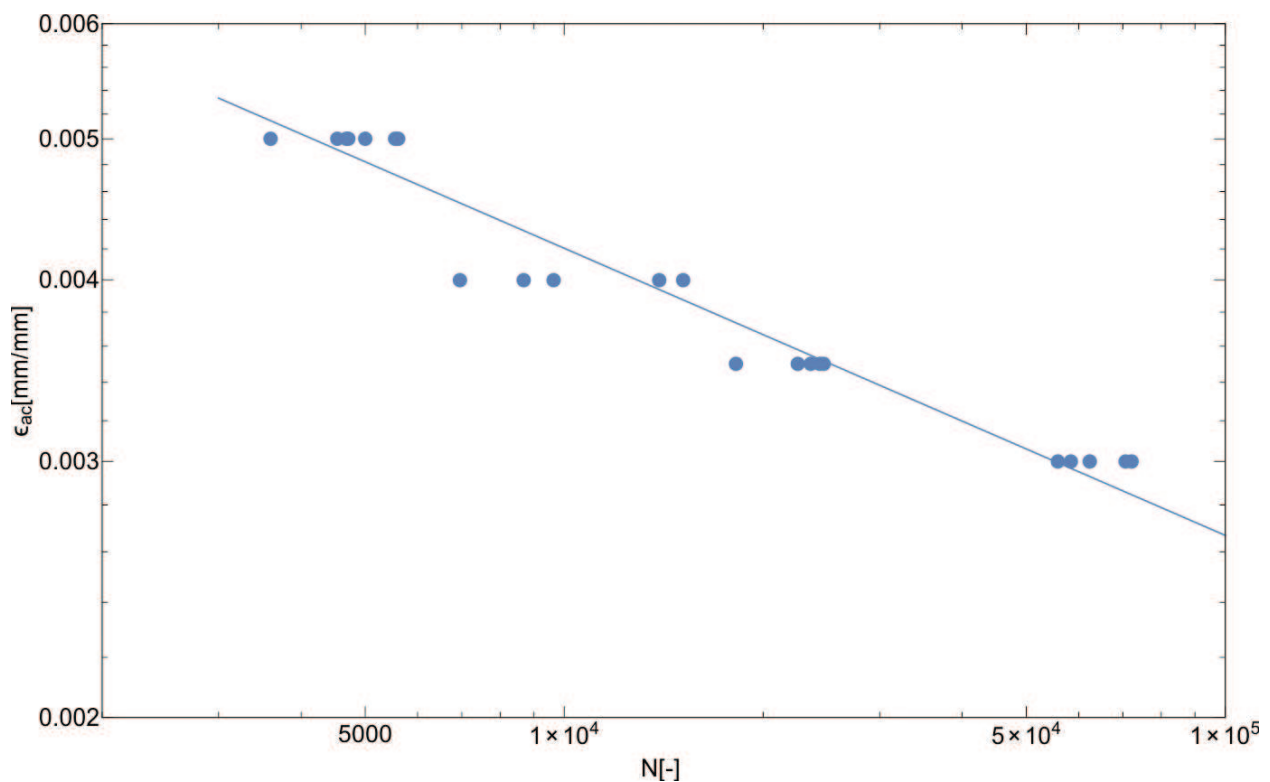


Figure 4. Measurement setup: (1) hydraulic pulsator MTS 810, (2) magnetic field measurement system, (3) extensometer, (4) magnetoresistor and (5) sample [18].

length. The used sensors are characterised by good measurement properties and a possibility to reduce the background field (the Earth's magnetic field and the field generated by steel objects surrounding the sensor). The accurate positioning of sensors and the method of conducting measurements are presented later in the paper.

The prepared measurement set was used to conduct low-cycle fatigue tests. The fatigue process was controlled by the total strain amplitude. The research was conducted for four thresholds,  $\epsilon_a = 0.003, 0.0035, 0.004$  and  $0.005$  mm/mm, respectively. Five samples were tested at each of the thresholds. The process was continued until a sample was broken. The load spectrum had a sinusoidal character ( $R = -1$ ), and the frequency was  $0.2$  Hz. The selected value of frequency counteracted the temperature growth resulting from material deformation, which prevented inverse transformation, That is, martensite  $\alpha' \rightarrow$  austenite  $\gamma$ .

**Figure 5** presents a low-cycle fragment of the Wöhler diagram. **Figure 6** presents results for a selected sample for input function  $\epsilon_a = 0.0035$  mm/mm. **Figure 6** presents the change of the area of the mechanical hysteresis loop and selected loops from the whole lifecycle of the sample. Moreover, some symbolic points corresponding with selected loops are marked in the figure. It is visible that the mechanical loop area decreases with the number of cycles, which confirms the strengthening of material when experimental control with total strain  $\epsilon_a$  is used. Before the tested sample broke, it had been loaded with  $N = 24,723$  cycles.



**Figure 5.** Low-cycle fragment of the Wöhler diagram [19].

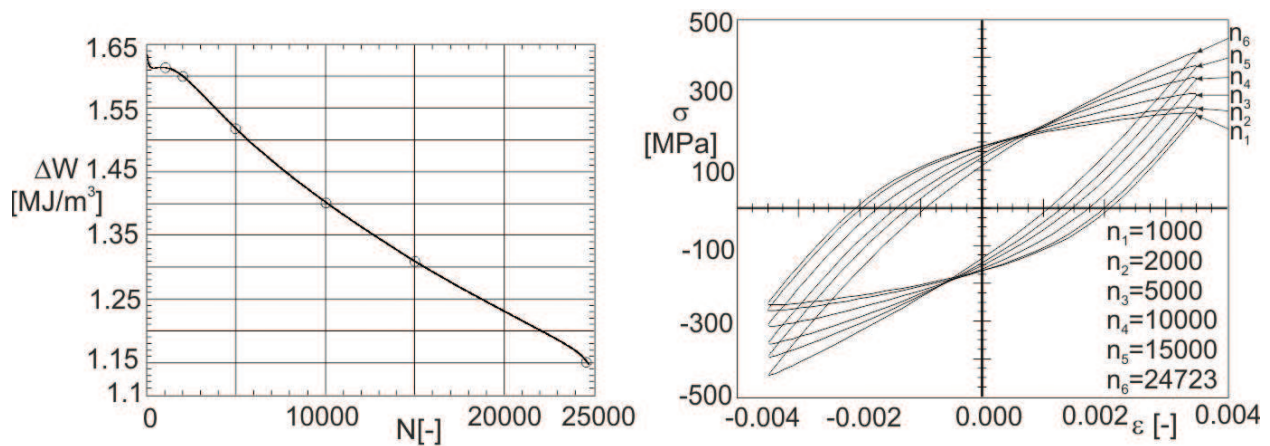


Figure 6. Area of the hysteresis loop with selected loops [19].

### 3.2. Methodology of magnetic measurements

#### 3.2.1. Preconditioning of magnetic measurements

Contactless measurement of magnetic field strength in the conditions existing during loading samples in a testing machine is a significant technical challenge [18, 20]. The measurements were conducted with a passive contactless method in which magnetoresistors were used as quasi-pointwise magnetic field sensors [13]. Before the experiment started, there were a number of conditions which had to be taken into account. The most important of them are briefly discussed below:

- a. Ensuring of non-magnetic surroundings around the tested sample is an ideal solution for passive methods. However, it is practically impossible due to the presence of a magnetic field. On the other hand, in the case of testing the separation of a martensite phase in paramagnetic austenite steels, the measurement signal is one order of magnitude smaller than the Earth's magnetic field [21].
- b. It is hard to eliminate the so-called 50 Hz magnetic field of electrical appliances.
- c. A hydraulic pulsator is made of numerous ferromagnetic parts that move during its operation. This means that the pulsator itself is a magneto-mechanical system. It was assumed that the introduction of interference in the machine system is pointless due to its ability to influence the correctness of performed fatigue loads. Moreover, irrespective of this, ensuring a zero magnetic field was unrealistic.
- d. The strongest magnetic field is related to the presence of strongly ferromagnetic wedges made of forged tool steel. Such a magnetic circuit is characterised by the opposite polarisation of the system of wedges along a sample, which is essential in the design of a measurement setup. The wedges have a knurled surface, which causes the permissible/acceptable collapse of the surface of a sample. An example of the influence of the knurled surface of the wedges is presented in a magnetic "picture" of an austenite steel sample that was taken with the author's original magnetovision camera (Figure 7) [21, 22]. There

are visible traces of the collapse caused by the knurled surface and the location of technological cutting of the sample. Hence, it can be observed that even only compressing the sample in the wedges leads to the local initiation of a magnetically strong martensite phase.

- e. The location of quasi-pointwise magnetic sensors with reference to the sample is important in the analysis of the magnetic circuit of the sample and the testing machine. The application of magnetoresistors is optimal due to the linear character of the response in terms of measurements and the very high sensitivity with relatively low noise. In the system of a typical Wheatstone bridge, these sensors are very sensitive measurement tools. For instance, when the signal is magnified about 1000 times, it is possible to record the process, through a wall from a distance of 10 m, the process of parking a car. In addition to this, these are wideband devices that can operate between a DC and AC signals at the frequency of a few MHz [23].

### 3.2.2. Position of sensors and the magnetic circuit of the sample and testing machine

The magnetic circuit of the sample and the testing machine, taking into consideration the above conditions, is presented in **Figure 8A**. Austenite sample **1** is fixed symmetrically in the strongly ferromagnetic wedges of the testing machine (top **2A** and bottom **2B**).

Two measurement devices are essential in mechanical measurements: extensometer **3** and force transducer **4**. The extensometer **3** with a specific measurement base (25 mm) is fixed symmetrically on the sample using special non-magnetic grips. The extensometer contains ferromagnetic parts in its construction (the so-called knives), and a small current flows through the device. However, it was assumed that placing the extensometer on the other side of the sample would not cause it to be a source of a significant interference field.

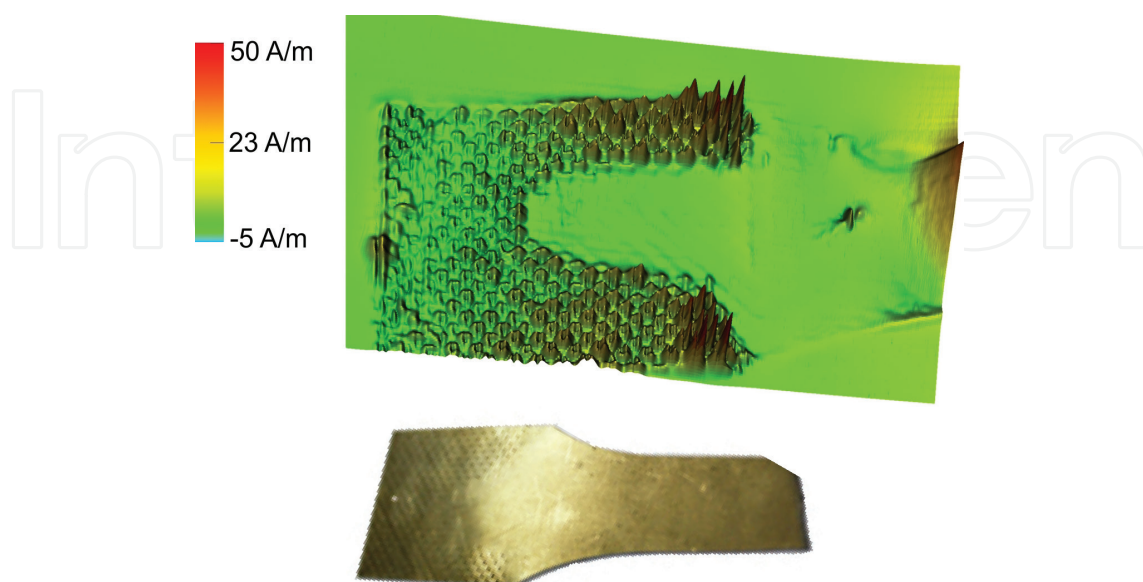


**Figure 7.** Visualisation of the magnetic field of the knurled sample AISI 304 compressed in the testing machine [21].



Taking into account the magnetic circuit of the testing machine and the sample, as well as the sensitive axis of magnetoresistors (along the sample, i.e. the y axis) distributed opposite the extensometer, the distribution of the magnetic field takes the N-0-S form, where “0” is the zero value of the field between the opposite poles N-S. N-0-S divides the sample into two influence zones of magnetic poles in which the zero line does not necessarily have to overlap with the sample axis of the symmetry axis. The measurement of the magnetic field is conducted in a contactless way at a small distance  $d$  (usually 1 mm) from the created surface of the cylindrical sample. The aspired goal is to locate the magnetic zero between sensors MR1 and MR4 and also between the extensometer knife edges. Due to the fact that the austenite steel sample is initially paramagnetic, the position of the zero line will be the only information that can be obtained from magnetic sensor indications. Only the separation of martensite will cause changes in signal value growth. Thus, the task to be completed by magnetic sensors was the online monitoring of the changes of the zero line position in particular loading cycles.

Due to the fact that the austenite steel sample is initially paramagnetic, the position of the zero line will be the only information that can be obtained from magnetic sensor indications. Only the separation of martensite will cause changes in signal value growth. On the other hand, fixing only one sensor on any part of the cylindrical sample will mean that measurements are taken at only one of the poles or will be possibly made in the not-very-advantageous area influenced by the magnetic zero line. The location of the sensor near the magnetic zero line may, in turn, cause its low indications.

Thus, it is more advantageous to design the measurement head 5 in such a way that there are two sensors distant from each other – there should be a small, constant distance “L” between them along the y axis, but simultaneously they must be located on both sides of the magnetic zero line. However, it is better to use a larger number of magnetoresistors. The reason for this is that internal sensors can follow the changes of the position of the zero line in particular cycles. Another solution is mapping the created cylindrical surface using a magnetic scanner (magnetovisual) that is synchronous with regard to the mechanical measurement value.

**Figure 8B** symbolically shows the course of magnetic field distribution changes along the sample related to the location of magnetic poles. Under the influence of a mechanical load, the sample is deformed. As a result of the Villari effect, a small change appears in the sample in the magnetic field distribution and is accompanied by the change of the zero line position on the sample. Such a process was described as the disturbance of the “magnetostatic balance” (in an ideal case, when martensite separations were uniform in each part of the sample micro-volume, the location of the magnetic field zero line would not change). This means that a change in the “magnetostatic balance” results solely from the presence of the martensite phase located randomly on the sample. The sensors conduct a certain kind of homogenisation by averaging their measurement surface. In consequence, the disturbance of the “magnetostatic balance” in the presence of a directed magnetic field can be treated as the measure of the quantitative content of martensite in austenite. In the next step, the key stage in the procedure of determining the amount of martensite in online monitoring of its content is obtaining the maps of zero line position changes.

The key assumption adopted below is that the linear range field changes along the sample near the zero line. Under the influence of a mechanical load, only the inclination of straight lines will change (apart from the earlier discussed position of the magnetic zero line) (**Figure 8B**).

The defined characteristic of the flux distribution allowed high-geometric-resolution maps showing the fluctuation of the magnetic field along the cylindrical sample to be prepared. These maps depend on the number of the load cycle, the index of this period (i.e. the angle in the period in the range of 0–360°) and the value of strain.

### 3.2.3. Methodology of magnetic measurements and their interpretation

The main task performed by the acquisition system of measurement signals, using MTS FlexTest GT, was recording the following variables in time:

1. Strain  $\varepsilon(t)$
2. Force  $S(t)$ , used to determine stress  $\sigma(t)$
3. Position of bottom grip piston  $R(t)$
4. Magnetic field strength  $H(t)$  in the form of four waveforms,  $H_1(t)$ ,  $H_2(t)$ ,  $H_3(t)$  and  $H_4(t)$ , respectively, obtained from a four-element head with sensors marked as MR1, MR2, MR3 and MR4

Due to the fact that magnetic measurements constitute a significant, technical challenge, the conducted research methodology described below presents the essential characteristics of the measurement head. Magnetic field acquisition is performed for sensors located on two opposite magnetic poles in the sample axis. The distance between the extreme sensors is small, typically 20 mm, which makes up 1/2 of the sample measurement part. The distance between the extremes of the magnetic field located in the poles, between the wedges, is at least five times bigger than the distance between two extreme sensors. The propagation of the magnetic field along the Y-axis in the place that is close to the magnetic zero can be interpreted as the zone of magnetic field linear increments with regard to sample length. The values of extreme sensors are not identical due to the fact that the position of the zero line is not known.

The magnetic field measurement head consists of four KMZ10 type magnetoresistors. Additionally, it is possible to make a head dedicated to various ranges of the geomagnetic field: for very weak magnetic fields of up to 200 A/m (KMZ10A, KMZ51), for medium ones of 1000 A/m (KMZ10B) and for strong ones of 10,000 A/m (KMZ10C).

Sensors from the KMZ10 family are standard magnetoresistor devices offered by NXP (previously Philips). They are characterised by a relatively big measurement area, thanks to which the level of value averaging per unit of length is significant. This, however, does not adversely influence measurements and is actually beneficial because the sensors are not sensitive to local geometric anomalies, that is, roughness, scratches and local martensite separations. These signals are more representative for the whole sample. Moreover, the ensured magnetic polarisation counteracts local magnetic anomalies, and as a result, sensor indications should be treated as “global” with regard to the magnetic zero line.

The process of setting sample load cycles was also conducted by using real-time control of the position  $R(t)$  of the bottom grip piston (when the top grip is immobile) in which the indications of the extensometer follow the profile

$$\varepsilon(t) = \varepsilon_{\max} \cdot \sin(\omega t), \quad (2)$$

at frequency  $f = 0.2$  Hz.

The fatigue process was registered until the sample broke. Throughout the whole time of the measurements, the sample was not elongated, which is essential with respect to immobile magnetic sensors.

The sampling of all measurement channels was conducted simultaneously at sampling frequency:

$$F_p = 360 \cdot f = 72 \text{ Hz}, \quad (3)$$

The synchronising period of the strain signal  $\varepsilon(t)$  was divided into  $i = 360$  equal time sections (period index  $i = 0, \dots, 359$ ) with consideration for the  $j$ 'th loading cycle  $n$ . Therefore, strains  $\varepsilon(t)$  were obtained as the functions of two variables  $\varphi_i$  and  $n_j$  connected with the period and the load index according to the following rule:

$$\varepsilon(\varphi_i, n_j) = \varepsilon_{\max} \cdot \sin\left(\frac{j \cdot 2\pi}{360} \cdot i\right), \quad (4)$$

The representation of a given value identical with  $\varepsilon$ ,  $\sigma$  and  $H$  can be analysed in the linear time increment (the so-called RAW, unprocessed data—an oscilloscopic course with a long-time basis) or with regard to the index  $i = 0$  of the forcing value, in this case  $\varepsilon$ . The model course of strain  $\varepsilon(\varphi_i, n_j)$  contains up-to-date information about the period index  $\varphi_i$  ( $i = 0, \dots, 360$ ). The course in time  $A(t)$  contained  $n_j$  cycles, where “ $j$ ” is the indicator of the load cycle period completed with breaking a sample. All measurement values ( $\varepsilon$ ,  $\sigma$ ,  $H_1$ – $H_4$ ) were synchronised with reference to index  $i = 0$  of the strain signal  $\varepsilon$ . The method of analysing the real signal waveforms of the magnetic field strength  $H(t)$  as RAW is shown in **Figure 9** on the example of four waveforms from the magnetoresistors (MR1, MR2, MR3 and MR4, respectively) that were fixed along the sample at equal distances from one another and in accordance with the scheme presented in **Figure 8**.

It should be noted that the signals in the counterphase from the MR1 and MR4 sensors are strictly correlated with semi-cycles of compression ( $\varepsilon_s$ )—tension ( $\varepsilon_R$ ). The analysis of magnetic field  $H(n_j)_{(\varphi_i)}$ , the maximum values for MR1 and the minimum values for MR4 refer to the same tension of semi-cycle; hence, all compression values ( $\varepsilon_s$ ) are in the waveforms in **Figure 9**.

The analysis of registered values, when only on the basis of their RAW-type time waveforms, is insufficient. It was necessary to develop methodology that would allow access to each registered value. The key aspect is the strain level  $\varepsilon(n_j)_{\varphi_i}$  for each synchronised measurement value in any load cycle until a sample is broken. This means that there is a possibility, due to the images being consistent with the linear increment of period index  $\varphi_i$  that is identified with the constant strain level  $\varepsilon$ , to build and further analyse the results using high-information-density graphic methods. Here, techniques known from the development of magnetovision,

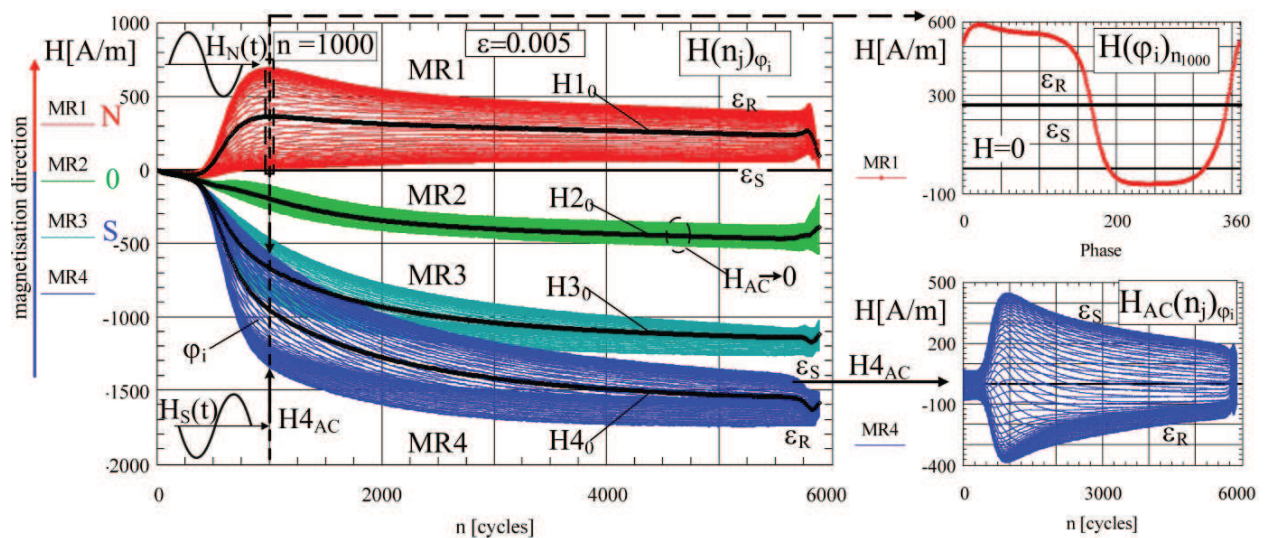


**Figure 9.** Example of the analysis of waveforms from the four magnetoresistors MR1, MR2, MR3 and MR4 located in accordance with **Figure 8**.

developed for many years by the authors of [21, 22], turn out to be especially useful. Recording values which are time synchronised with one another allows the drawing of maps and tomograms based on period index  $\varphi_i$  or load cycle  $n_j$ , defined as phase maps (2D) and tomograms (3D). It resembles the decomposition of an analogue TV signal transmitted as a time waveform to an image form in which a frame is a kind of two-dimensional map [24]. Additionally, the term phase means here that the maps are mainly used to determine phase shifts (phase-sensitive detector) with reference to the model that is the strain map  $\varepsilon(\varphi_j, n_j)$ . The maps can comprise of even several millions of points, which is an essential parameter in typical data analysis as it was shown charts [25]. The assumed map size usually has the dimensions of table 2D  $360 \times j_{\max}$ . In this way it is possible to conduct the imaging of various physical values, mapped with reference to the increment of a given parameter [26–28]. In the case of the martensite transformation, the main focus was on strain, stress and magnetic field maps.

**Figure 10** presents the phase maps  $H(\varphi_j, n_j)$  for the MR1 and MR4 sensors of a sample loaded with a profile with the maximum amplitude of total strain  $\varepsilon_a = 0.005$ . On the map level, lines mark the ranges of similar values of a magnetic field. The cross sections along indexes  $(i, j)$  allow waveforms as cycle periods, and also changes occurring under the influence of the fatigue process, to be obtained. **Figure 10** presents selected period waveforms for load cycle index  $j = 100$  (1200th cycle of sample loading) with marked maximum and zero values ( $i = 80, i = 170, i = 260$ ). The changes of a magnetic field under the influence of the fatigue process are presented for index  $i = 20$ .

The results in the form of maps are the basic tool in the cognition of the martensite transformation phenomenon and also an interface that allows image processing methods known from machinery visioning (MV) or DIC techniques [29] to be used.

The key assumption made by the authors is the linear range of field changes along the sample near the zero line. Under the influence of a mechanical load, only the inclination of straight lines along the sample, related to the propagation of the field, will change, as shown in **Figure 8B**.

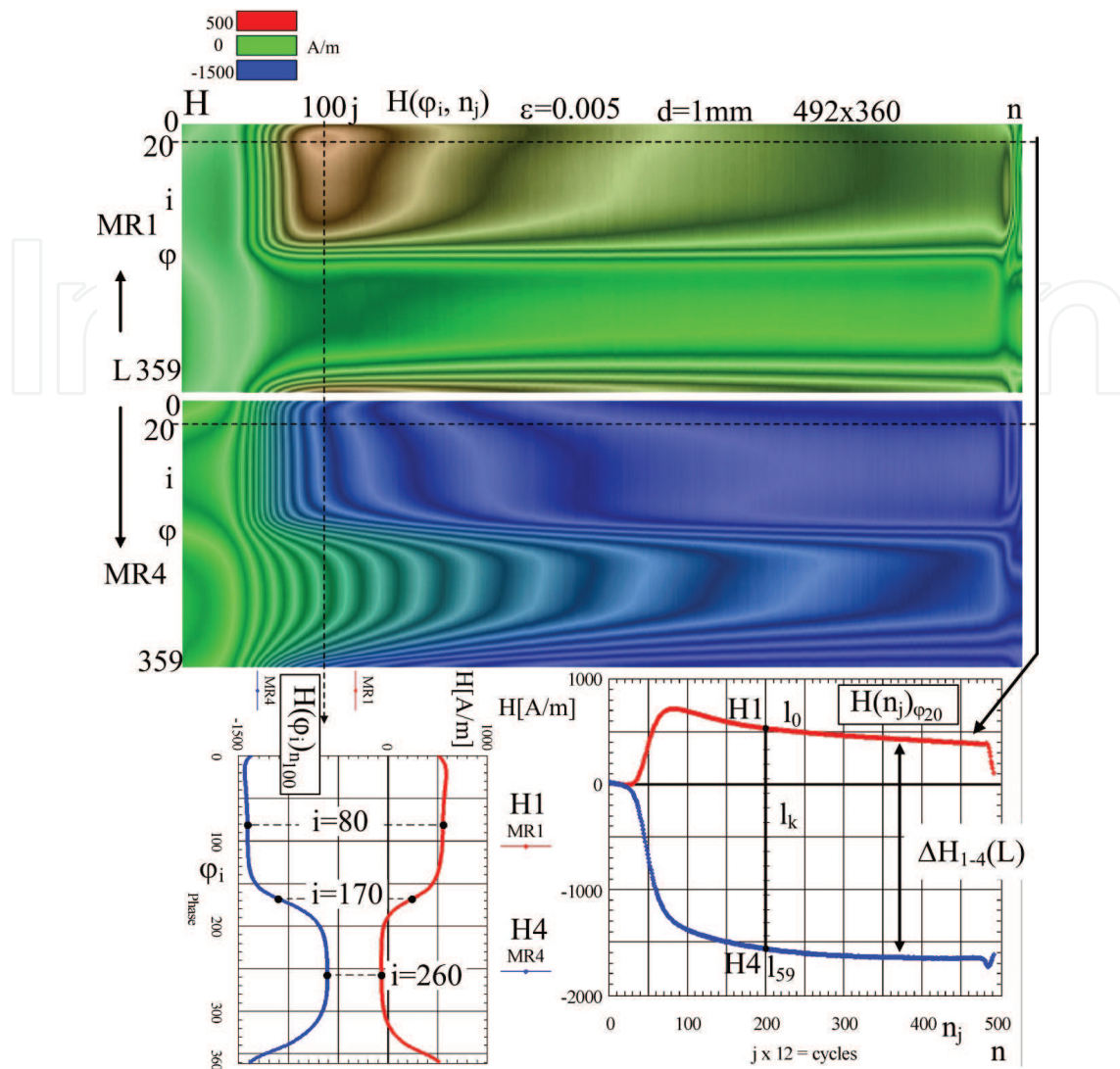


**Figure 10.** Phase maps for MR1 and MR4 sensors for the sample loaded with profile  $\epsilon_a = 0.005$ .

Thanks to this assumption, it is possible to develop high-geometric-resolution maps that show the changes of a magnetic field along a cylindrical sample depending on a given load cycle and its period index (the angle in period in the range of 0–360°), related to a current strain. The  $H$  maps  $(\varphi_i, n_j, l_k)$  obtained for sample  $\epsilon_a = 0.005$  are presented in **Figure 11**. The level lines mark the ranges of similar values of a magnetic field for the same angle in period (phase index).

It was said earlier that the position of a sensor on the sample is essential because of the distance from the unknown position of the zero line. Any attempt to interpret a signal from a single sensor is influenced by its position with reference to the zero line of a magnetic field [30]. For the purpose of gaining independence of the zero line position, the operation of the determination of the increment of magnetic field strength depending on sample length  $H'$  must be conducted:

$$H'(\varphi_i, n_j) = \frac{dH(\varphi_i, n_j, l_k)}{dl}, \quad (5)$$

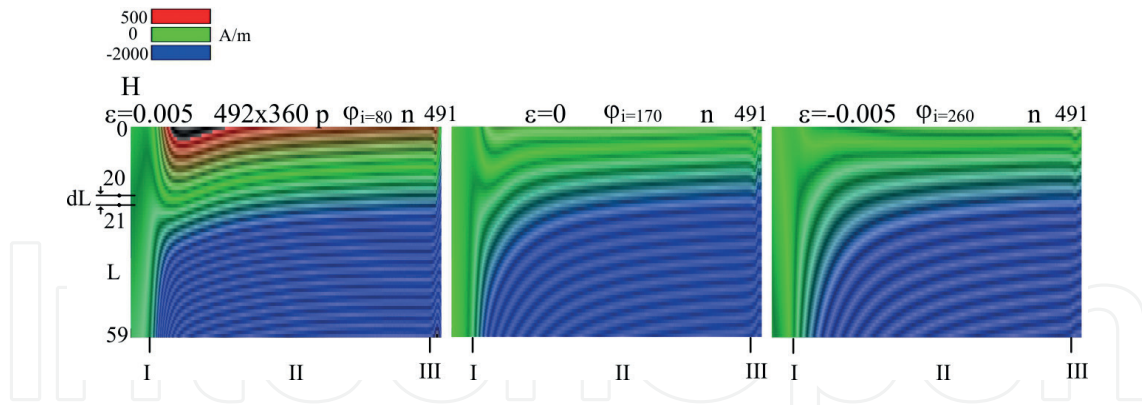


**Figure 11.** Magnetic field distribution maps used to determine zero line ( $H = 0$ ) position changes under the influence of the number of cycles with regard to a set phase index.

The method allows for the consequences of some imperfections in the course of the fatigue process to be compensated, for example, minor sliding of extensometer knife edges or minimum sample elongation. **Figure 12** presents waveform  $H'$  with marked envelopes of maximum values,  $H'_{max}$  and  $H'_{min}$ , respectively. **Figure 13** presents a phase map with corresponding cross sections. Special attention should be drawn to the waveform of averaged value  $H'_0(n_j)$ , which is a characteristic value for the whole sample and depends only on the load cycle. Hence, all measurement results in the form of individual sensor waveforms, or maps can be reduced to the average value of magnetic field increment along path  $H'_0$ . Waveforms  $H'_0(n)$  characterise the accumulation of martensite emitted in a sample during a fatigue process, with a set level of strain amplitude  $\epsilon_a$ .

### 3.3. Application of the magnetic field increment method in martensite content assessment

Average magnetic field increment per unit length of the measurement part of sample  $H'$  was assumed to be the magnetic measure of the martensite phase content in a sample. The strain

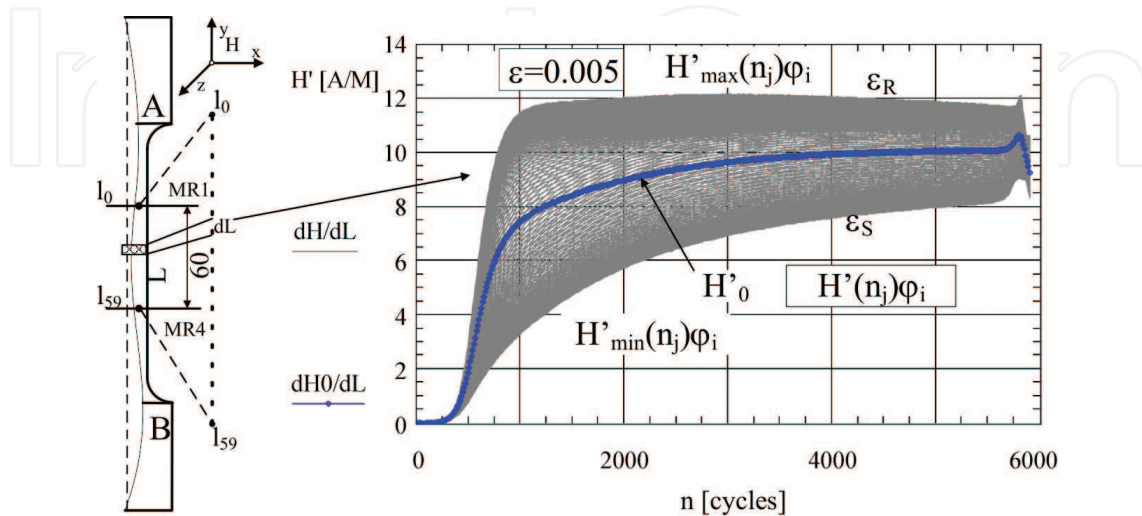


**Figure 12.** Waveforms of changes  $H'(n)$  depending on load cycle for set  $\epsilon_a$ .

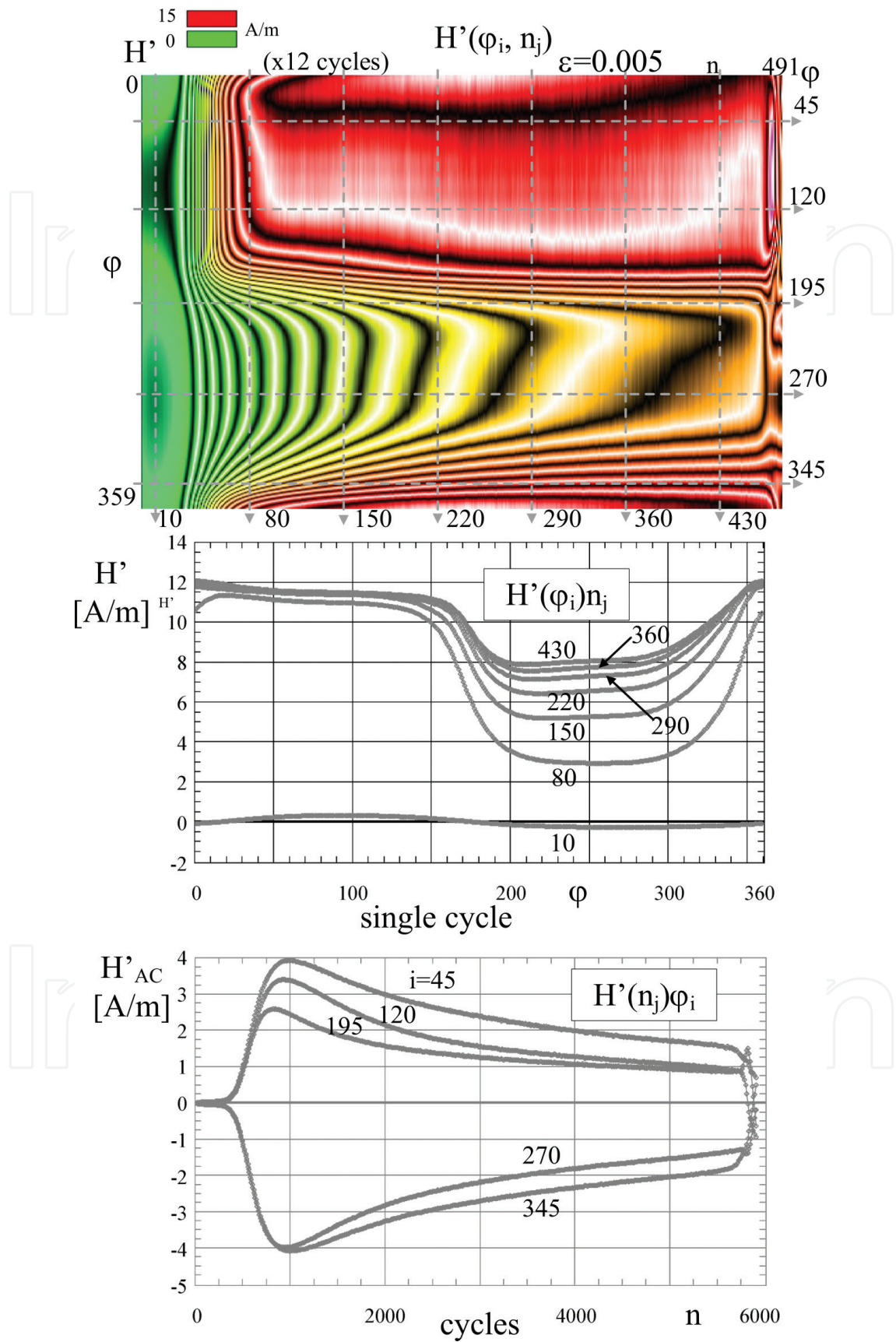


Figure 13. Map of changes in the increment of magnetic field  $H'$  synchronised in period  $\varphi$  and load cycles for set  $\varepsilon_a$ .

level  $\epsilon_a = 0.005$  was the maximum level at which sample geometry did not change until the sample broke. The reason for this is that in earlier research it was shown that for  $\epsilon_a = 0.0055$ , buckling took place very quickly. As a result, the value of  $\epsilon_a = 0.005$  was assumed to be the critical  $\epsilon_k$  to which the results would refer, especially when the high repeatability of results for mechanical and magnetic values was detected.

The analysis of these waveforms allowed the so-called maximum amount of martensite  $V_H$  with regard to the highest strain values ( $\epsilon = 0.005$ ) to be determined:

$$V_H = \frac{H'_0(n_j)(\epsilon_a)}{H'_0(n_j)(\epsilon_k)} \cdot 100\%, \tag{6}$$

**Figure 14** shows waveforms  $H'_0(n_j)$ , depending on the strain level, for three samples of various total strain levels with value  $V_H$ . The error in the results for the method is connected with the quotient of the critical total strain and the strain at which the sample buckles, in this case  $\delta V_M = \frac{0.005}{0.0055}$ , i.e. about 10%.

In **Figure 14**, value  $V_H$  is also marked and is related to the number of sample loading cycles before the sample breaks and the increment of magnetic field  $H'_0$ , which is the measure of accumulated martensite content. The next step will be scaling values  $V_H$  in the same way as the accumulated martensite content in a fatigue process using optical microscopy or roentgenographic methods. The analysis of subsequent values  $H'_0(n_j)$  with regard to the load cycle index allows the determination of the martensite increment speed, which can take the following form:

$$H_0'' = \frac{H'_0}{dn}(n_j), \tag{7}$$

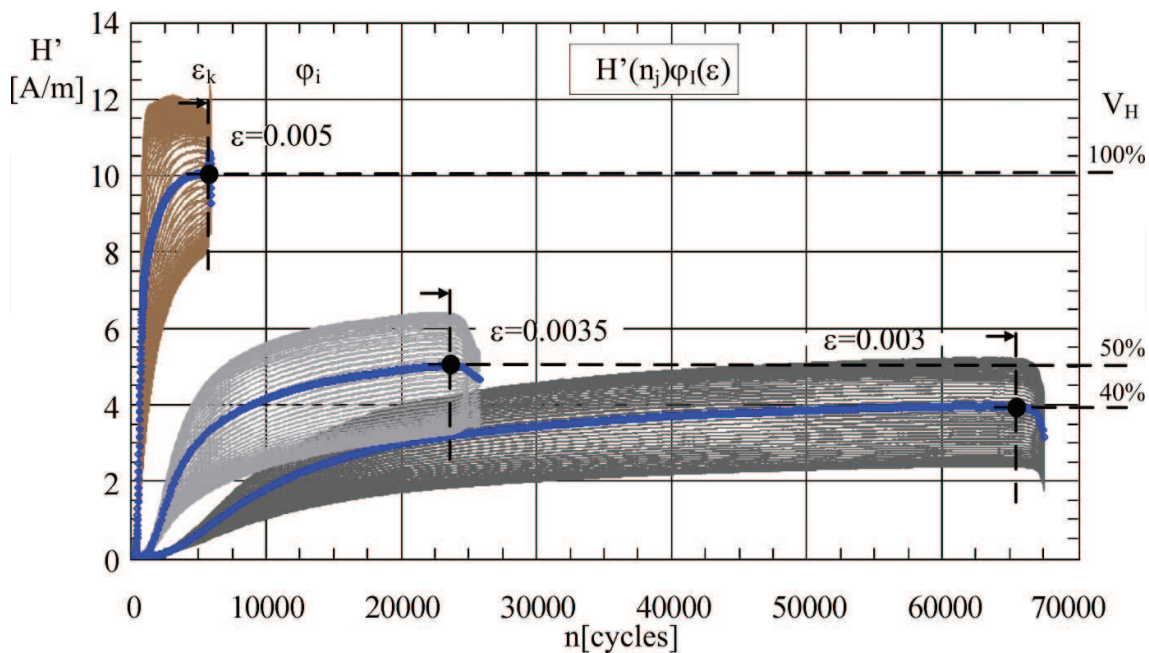


**Figure 14.** Comparison of  $H'(\epsilon)$  with the number of load cycles for three load levels.

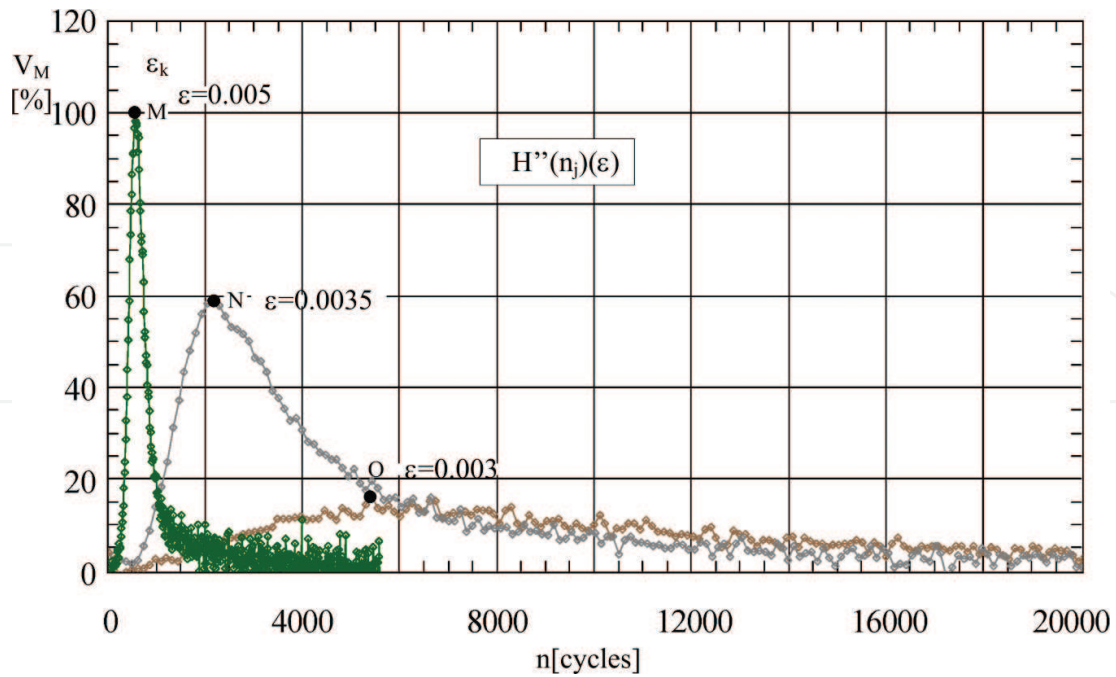


Figure 15. Relative martensite increment speed marked as  $V_M$  depending on the level of total strain  $\epsilon_a$ .

With reference to the critical value of the total strain level  $\epsilon_k$ , it can be stated that

$$V_M = \frac{H_0''(n_j)(\epsilon_a)}{H_0''(n_j)(\epsilon_k)} \cdot 100\% \quad (8)$$

In Figure 15,  $H''_{max}$  points are marked as the maximum speed values of the martensite phase occurrence with regard to the sample with the critical strain level.

#### 4. Application of the thermo-elastic effect: measurement methodology and analysis of results

Temperature was measured using a type E thermocouple made in a classical manner using two wires (CuNi and NiCr) with a diameter of  $d = 20 \mu\text{m}$  each. The small mass of wires reduced thermal inertia and enabled the registration of the higher harmonic components of temperature signal  $\Delta T(\xi)$ .

The basic parameters of the thermocouple used in the measurements are presented in Table 2.

In the measurements, a universal measurement system consisting of a spectrum analyser HP E1432A and the Keysight VEE software package was used.

Figure 16 presents the cyclic stress-strain curve  $\sigma_a - \epsilon_a$  for the tested material. The cyclic yield limit is  $\sigma_a = \sigma_{cpl} = 326 \text{ MPa}$ , and the corresponding value of strain amplitude is  $\epsilon_a(\sigma_{cpl}) = 0.0016$ . The curve was determined by connecting the peaks of subsequent hysteresis loops at gradually incrementing load levels. The hysteresis loops are also presented in Figure 16. Above

| Notation | Materials |      | Voltage value change to °C depending on temperature |          |           | Range of thermocouple work in °C |                | Thermocouple tolerance |                |
|----------|-----------|------|---|----------|-----------|----------------------------------|----------------|------------------------|----------------|
|          |           |      | 100 [°C]  | 500 [°C] | 1000 [°C] | Continuous work                  | Temporary work | -40 ÷ 375 [°C]         | -40 ÷ 375 [°C] |
| E        | NiCr      | CuNi | 68  | 81       | -         | 0 ÷ 800                          | -40 ÷ 900      | ±1.5                   | ±0.004* t      |

Table 2. Basic parameters of type E thermocouples.

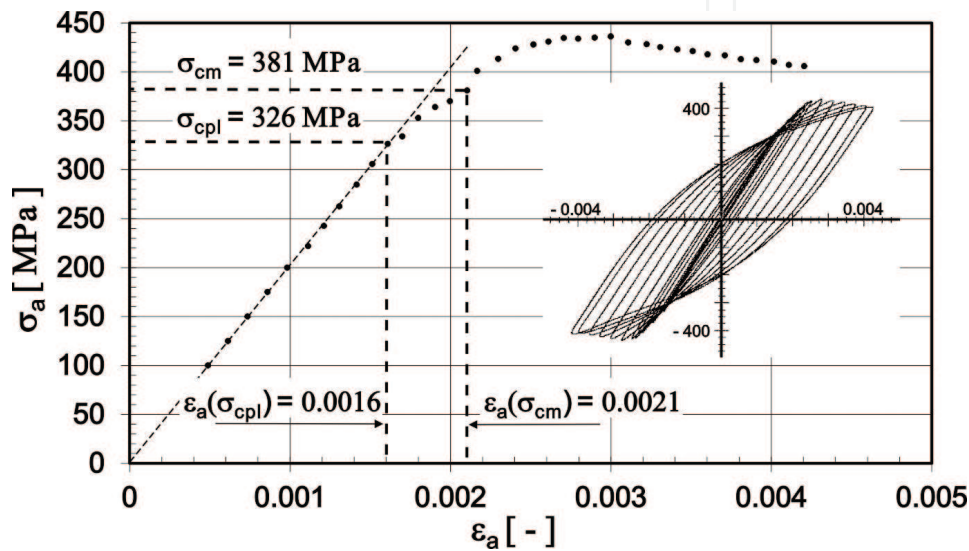


Figure 16. Cyclic stress-strain curve  $\sigma_a$ - $\epsilon_a$ .

the cyclic yield limit, it is possible to observe a characteristic fault on curve  $\sigma_a$ - $\epsilon_a$ , which was identified with the cyclic limit of the martensite transformation  $\sigma_{cm} \approx 380$  MPa (corresponding with strain amplitude  $\epsilon_a(\sigma_{cm}) = 0.0021$ ).

Temperature signal  $\Delta T(\xi)$  underwent harmonic analysis using the fast Fourier transform (FFT). In the further part of the analysis, the subsequent sinus components of signal  $\Delta T(\xi)$  were marked as  $1_{sin}, 2_{sin}, 3_{sin}$ , etc., whilst the cosine components were marked as  $0_{cos}, 1_{cos}$ , respectively, etc. **Figure 17** presents the change of average temperature value  $\Delta T_m(\epsilon_a)$ , which is equivalent to the waveform of the zero cosine component  $0_{cos}(\epsilon_a)$ .

Temperature value  $\Delta T_m$  is equal to zero until the strain reached the value  $\epsilon_a = 0.0016$ , which corresponds to the cyclic plasticity limit ( $\sigma_a = \sigma_{cpl} = 326$  MPa). Later, temperature  $\Delta T_m$  systematically grows with the increase in strain and, hence, also plastic strain. In **Figure 17**, the initiation moment of the martensite transformation is also marked; however, there is no particular visible trace of this moment in transform  $\Delta T_m(\epsilon_a)$ . **Figure 18** presents the set of harmonic components (ignoring  $0_{cos}$ ) as a load-level function.

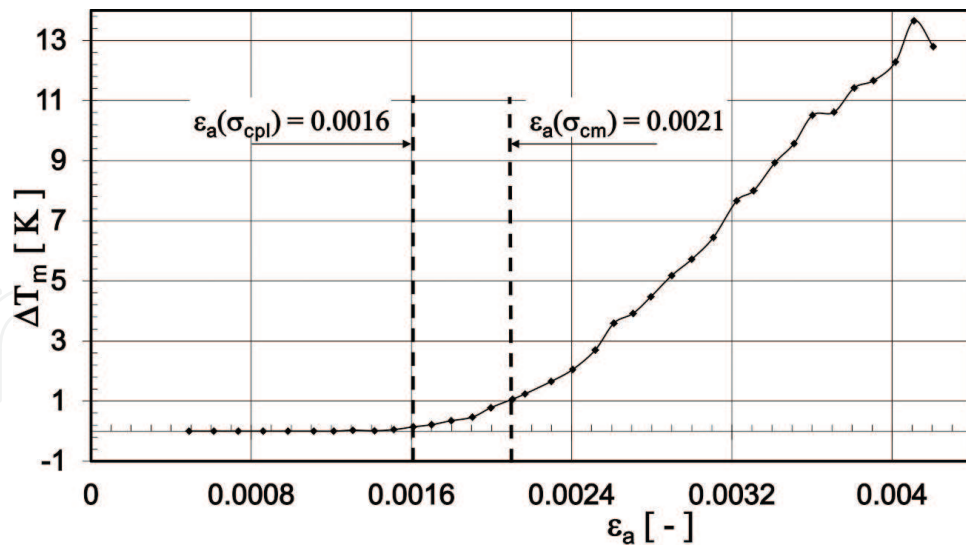


Figure 17. Average temperature dependence on the strain amplitude level  $\Delta T_m(\epsilon_a)$ .

In the area in which only the thermo-elastic effect occurs, one can easily observe that the first sinus component ( $1_{sin}$ ) is linearly dependent on the load level until the cyclic plasticity limit occurs. The influence of higher harmonic components in the elasticity region is negligible.

After crossing the cyclic yield limit, one can observe the deviation of experimental waveform  $1_{sin}$  from the linear one, and there are also higher harmonic components. Thus, **Figure 18** confirms the fact that the Thomson model is correct in the elastic range of a paramagnetic material.

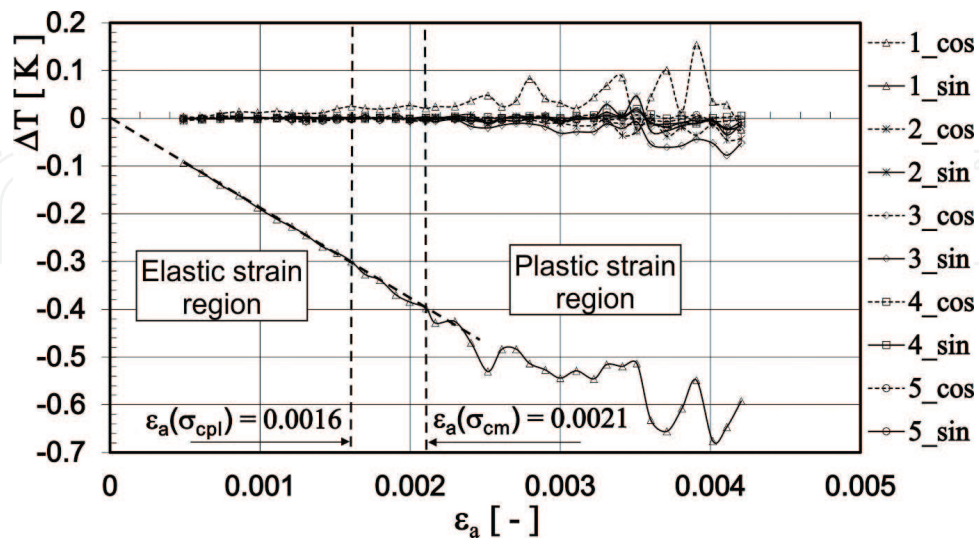


Figure 18. Harmonic components (cosine and sinus) of temperature signal  $\Delta T(\xi)$  as a function of strain amplitude  $\epsilon_a$ .

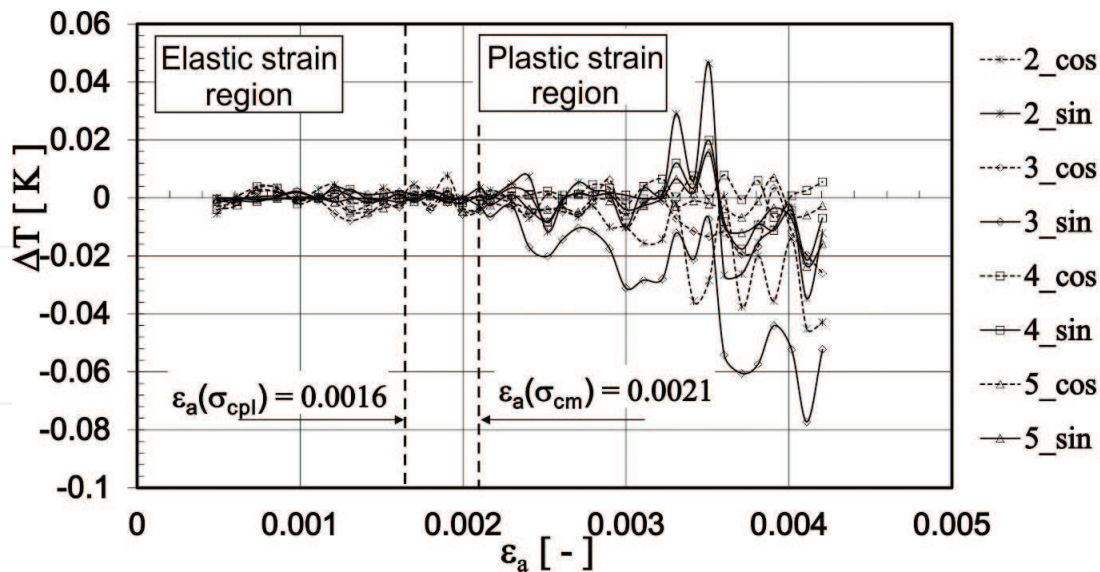


Figure 19. Harmonic components (cosine and sinus) of temperature signal  $\Delta T(\xi)$  as a function of strain amplitude  $\varepsilon_a$ .

Higher harmonic components (except  $1_{sin}$ ,  $0_{cos}$  and  $1_{cos}$ ) are presented in Figure 19. The effect of the so-called saddle effect, analysed earlier in Figure 1, is visible here in the form of a clear increment of higher harmonic components, especially the second and fourth expression.

## 5. Research on the martensite transformation induced by plastic deformation in austenitic foils

The way of investigating the kinetics of the martensite transformation induced by plastic strain in austenite foil of 0.05 mm is presented below. The problem is discussed in detail in [31, 32].

### 5.1. Preconditions of the measurements of martensite transformation kinetics in austenite foils

The research on materials in the form of a thin foil is a challenging task in terms of conducting measurements. It is necessary to take into consideration the following conditions and requirements:

- a. The small size of samples (the cross section of the investigated part in the analysed example was  $0.195 \text{ mm}^2$ , that is, about 290 less than in the case of the cylindrical sample). This means that force must be applied with an accuracy of 0.1 N. The way of fixing a sample, controlling load and recording measurement signals, both mechanical and magnetic ones, is also of key significance.
- b. The necessity to eliminate the negative impact of the magnetic background of a standard magnetic pulsator and to conduct structural research on line (during loading samples) meant that it was necessary to build a miniature testing machine. The small dimensions of the machine and its mass below 1000 g allowed the experiment to also be conducted in the vacuum chamber of a scanning microscope.

- c. The need to measure magnetic field strength so as to detect the initiation and increment of ferromagnetic martensite  $\alpha'$ . Small increments  $\Delta H$  required the elimination of field disturbances resulting from both the flow of electric current through the extensometer and the subcomponents of the testing machine made of a ferromagnetic material.
- d. Creating dumbbell-type samples of foil required the construction of a special blanking tool which minimised plastic strains on sample edges and, hence, also the initiation place of the martensite transformation. Additionally, samples were tempered using a special procedure.
- e. The necessity to eliminate the negative impact of the magnetic background of the standard hydraulic pulsator meant that it was necessary to construct a miniature testing machine.

## 5.2. Research object, measurement setup, methodology and experiment results

The material was delivered in the form of foil, 0.05 mm thick, in the state marked by the manufacturer as  $1/8 \div 1/4$  of hardness. The foil was heat treated for the purpose of recrystallisation. During the treatment the sample was heated to oversaturation temperature, that is, about  $1050^{\circ}\text{C}$ , and next it was quickly cooled down in air.

After the process of the mechanical cutting of the sample, it was heat treated one more time at a temperature of  $1100^{\circ}\text{C}$  for about 4 s and then cooled down in air. Due to the small size of the samples, they were heated up to a temperature of  $1100^{\circ}\text{C}$  using the flow of electric current of the previously set, experimentally selected parameters. The heat treatment of the samples was conducted on a test setup specially created for this purpose, which consisted of a voltage source (autotransformer) and measurement devices to control temperature, current and voltage.

The conducted heat treatment allowed the obtaining of a single-phase, paramagnetic material with austenite structure, which was free from residual stress, martensite and most dislocations. The average size of grain after annealing was about  $40\ \mu\text{m}$ . For the purpose of removing the created in the process magnetic oxides covering the surface of samples, they were polished electrolytically before the research until they were  $80\ \mu\text{m}$  thick. The structure of the material when it was delivered and after heat treatment is presented in **Figure 20A** and **B**.

The shape and dimensions of the sample are presented in **Figure 21**.

The main subcomponent was the miniature testing machine (micro-tensile testing machine) presented in **Figure 22**.

Loads were applied using a system with a precise lead screw, worm gear and numerically controlled stepper motors. The drive allowed grips to be shifted in a speed range between  $0.095\ \text{mm/min}$  and  $0.0005\ \text{mm/min}$ . The other system ensured transverse movement allowing a sensor to be relocated. This measurement system enabled the recording of mechanical signals (force  $S(t)$ , displacement  $\Delta l(t)$ , strain  $\varepsilon(t)$ ) and changes in magnetic field strength  $\Delta H(t)$  [23, 33]. Signal processing was conducted using the VEE measurement package and MATLAB.

The determination of the quantitative content of a martensite phase in a material is important, for example, in selecting the technological parameters of plastic forming or welding processes.

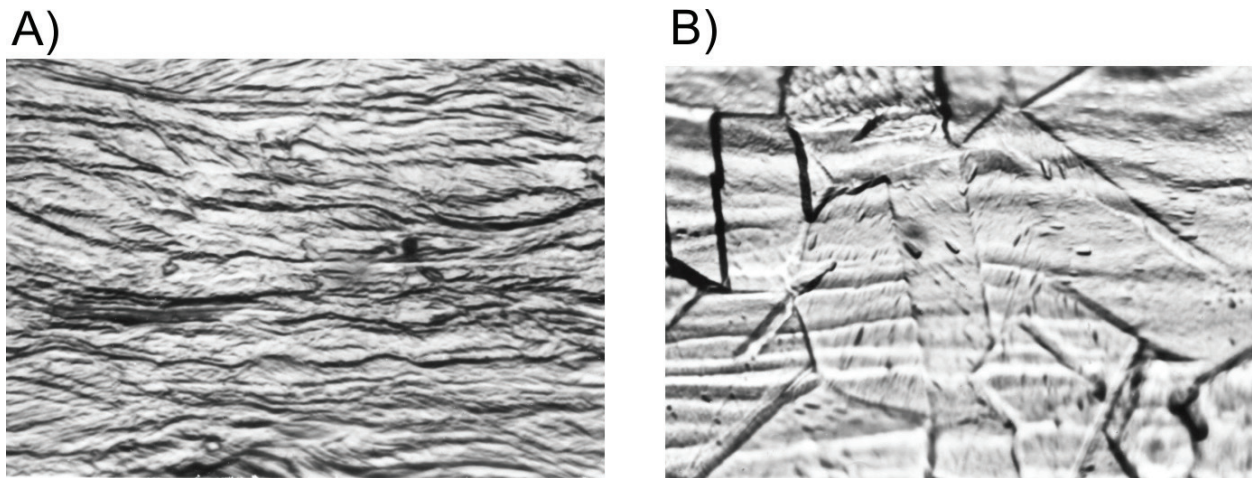


Figure 20. Structure of AISI 304 steel (1000× magnification): before heat treatment (A) and after heat treatment (B) [31].

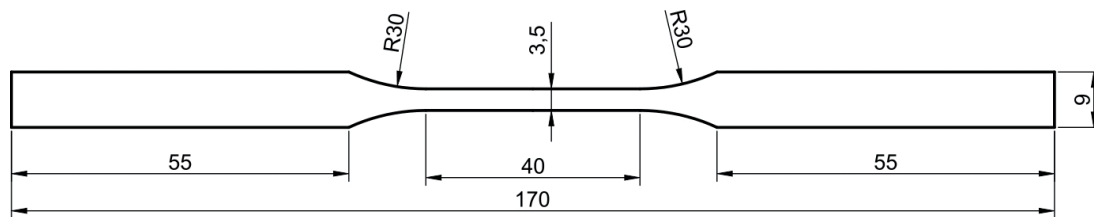
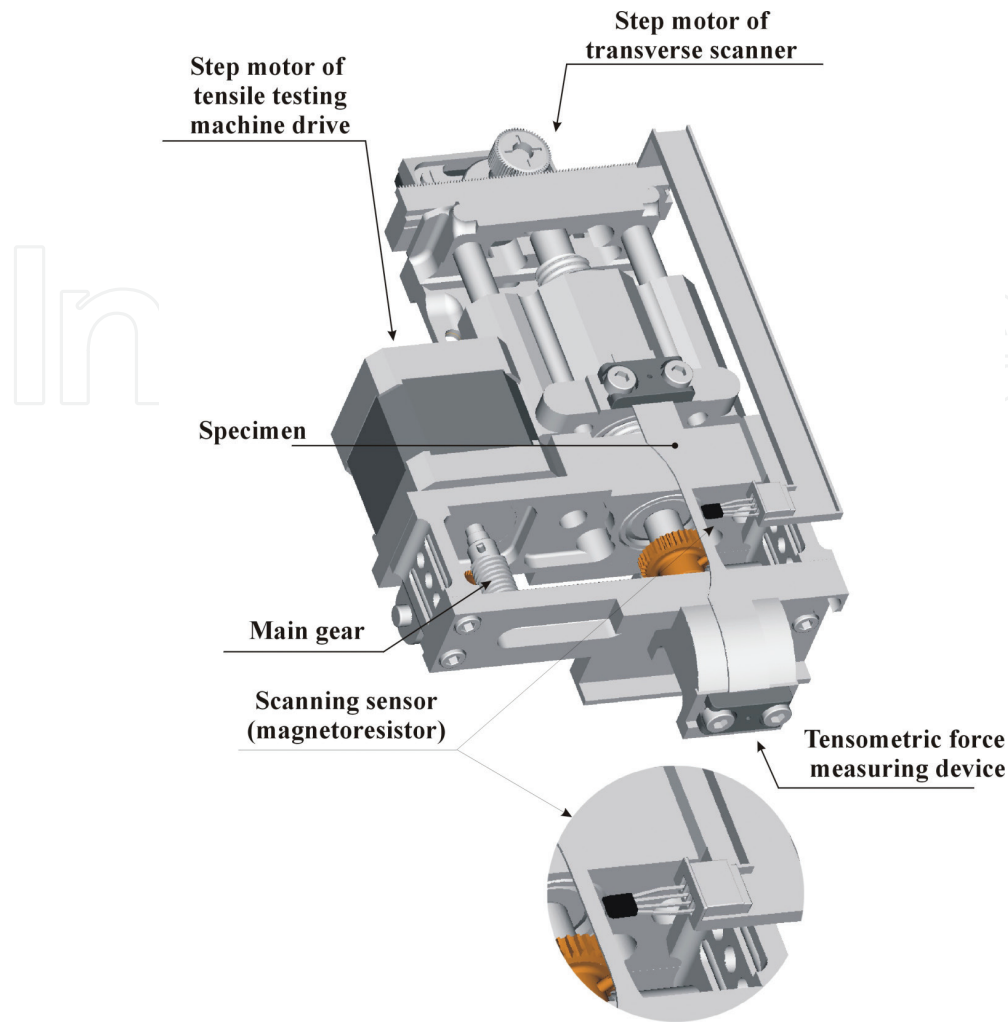


Figure 21. Sample shape and dimensions [31].

There are methods that allow the content of the martensite phase to be determined in laboratory and industrial conditions. Destructive tests encompass:

- Optical microscopy, for example, using phase contrast
- Electron microscopy, using a scanning electron microscope (SEM)
- Roentgen methods

One of the most effective methods of determining the amount of residual austenite in steels is the roentgen method. It examines the mutual intensity ratio of X-ray reflections, in particular phases, which were diffracted on the crystalline network of the examined steel. X-rays are diffracted on crystalline networks at various Bragg angles. This allows identification of these phases in steel and calculation of their percentage content, including also residual austenite. This is why the research was conducted using both the magnetic method and a diffractometer. The measurements were made using the test setup based on the micro-tensile testing machine. During the work, it turned out that the sensitivity of magnetic sensors was high enough to also register the movement of the mechanism in the miniature testing machine. As a result, a mobile measurement beam made of aluminium and a sample with a dynamometer system were located at a significant distance from the ferromagnetic parts of the micro-tensile testing machine. An important source of interference turned out to be the tensometric bridge of the dynamometer, the problem of which was solved by using lower voltage than before. As



**Figure 22.** Construction of the micro-tensile testing machine with a description of its main components [31].

a result of these actions, at least a 10-fold lower influence of the interfering magnetic field in the background was obtained, which enabled the high resolution of magnetic field increment measurement 0.01 A/m.

The tested foil was placed in non-magnetic grips, and the controlled process plastic strain was started. **Figure 23** shows the pictures of austenite foil fixed in the grips of the measurement device in which it was broken.

**Figure 24** presents the tension curve (A) and its magnetic response (B) for the tested austenite foil. The increase in magnetic signal was the consequence of the appearance and increase in martensite  $\alpha'$ , a ferromagnetic material in the paramagnetic austenite matrix.

The tests on foil were also conducted using an Xstress 3000 diffractometer. The sample was exposed to radiation at various values of strain. The obtained results are presented in **Figure 25**. The Y-axis is the intensity of X-ray captured by the matrix CCD on which there is a beryllium screen transmitting only a particular wavelength of radiation. The X-axis is the CCD matrix resolution.

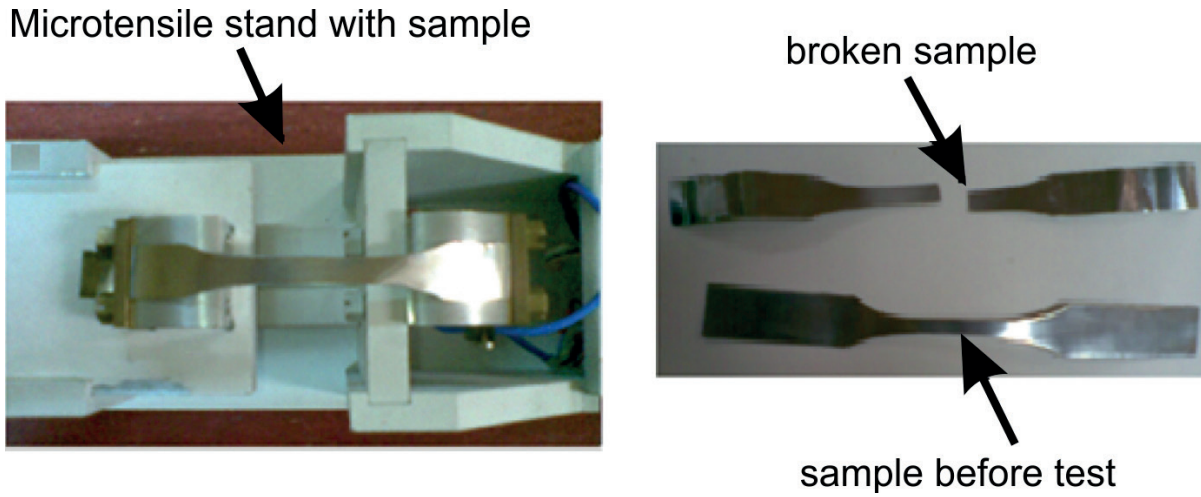


Figure 23. Thin austenite foils: sample fixed in the grips of the micro-tensile testing machine, sample before measurement and after breaking [31].

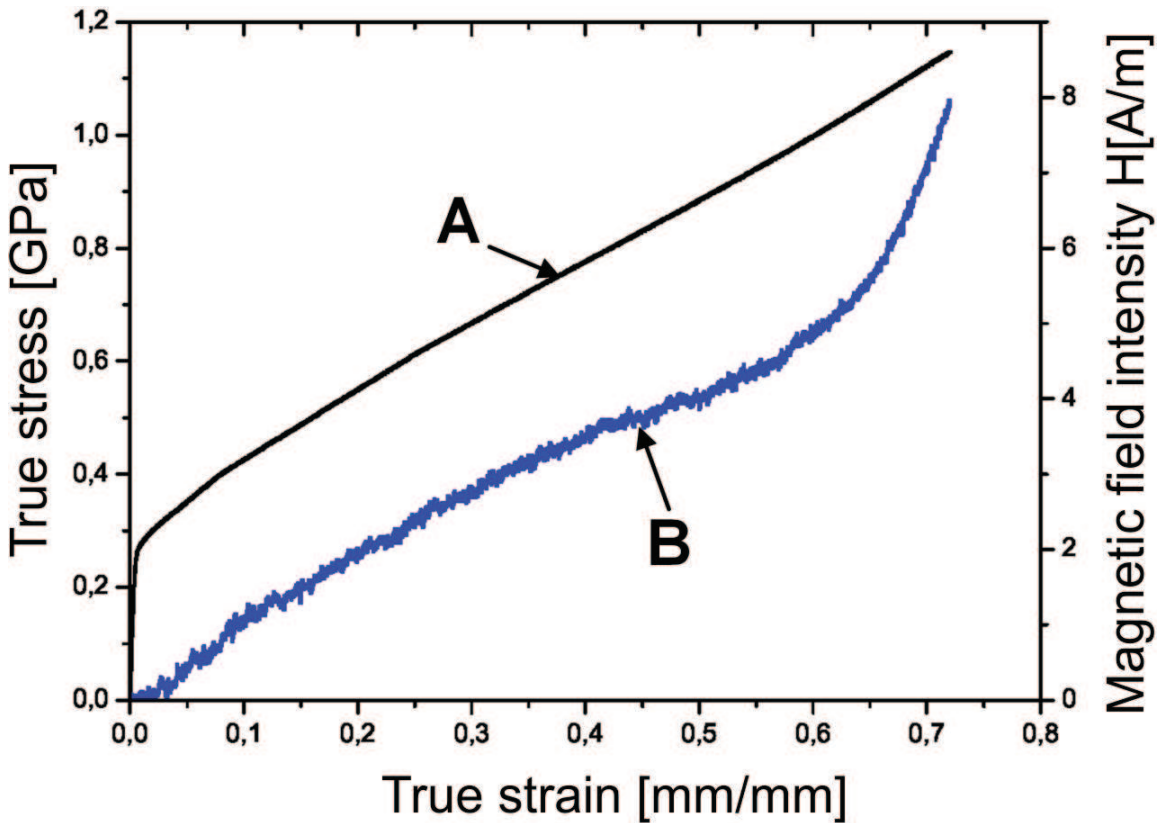


Figure 24. Results of plastic strain of the austenite foil sample: quasi-static stress-strain curve of the material and magnetic response to plastic strain [18].

As was demonstrated before, the changes of the magnetic properties of a material resulting from its strain are strictly related to the kinetics of the examined martensite transformation induced by plastic strain [31, 32]. It was shown in earlier works [32] that the first martensite nuclei appear after exceeding  $\epsilon = 0.035$ , which is recorded by both magnetic field sensors and an Xstress 3000 diffractometer.

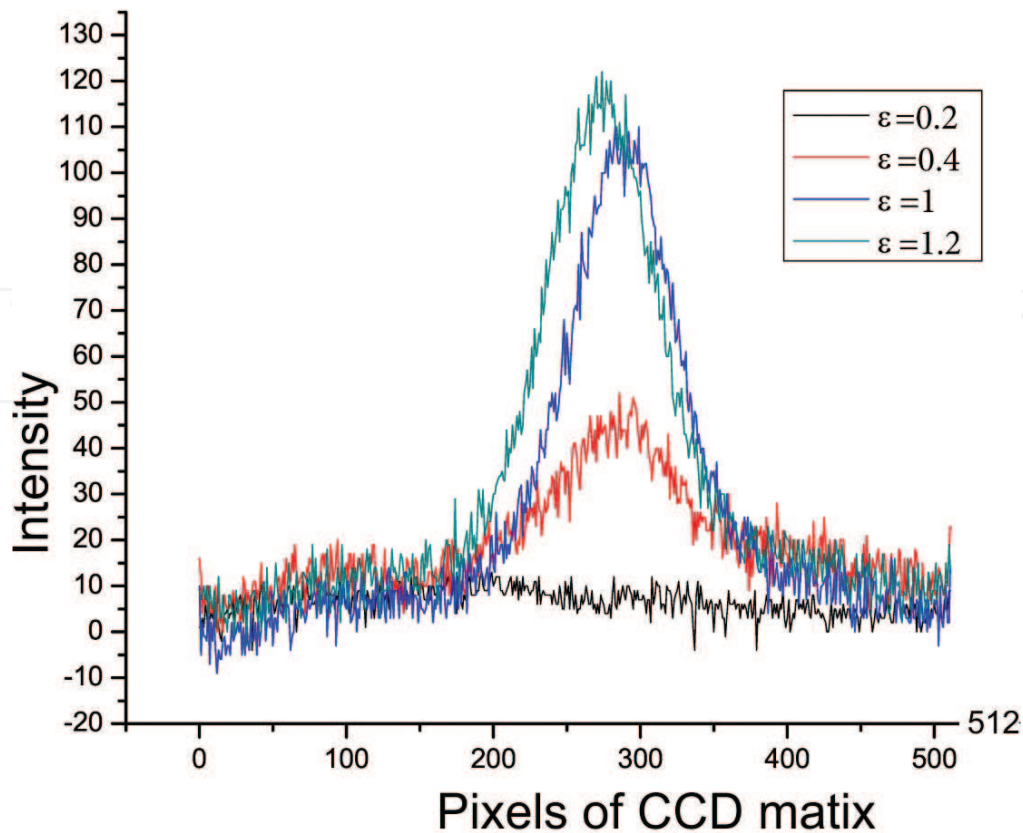


Figure 25. Images obtained from the CCD matrix: spectrum intensity change for selected strain levels [18].

Foil samples were loaded at the speed of 0.035 mm/min. In the introductory phase of each experiment, the goal was to achieve initial stress so as to eliminate the corrugation of the sample. Next, the main part of the experiment was conducted until the sample was broken. Mechanical magnetic signals were recorded all the time.

Figure 26 presents the experimental dependencies of force  $S(t)$ , strain  $\epsilon(t)$  and magnetic field strength  $H(t)$ . It should be emphasised that the strain signal could only be measured to the value of  $\epsilon \approx 0.0012$ , and after reaching this value the sensor was destructed.

The analysis of signals in the initial phase of strain is clearer if waveforms are presented, for example, until time  $t = 16$  minutes, which is presented in Figure 27. It is then possible to distinguish a few phases of the process. The first stage takes place in the time range  $0 \leq t \leq 3.7$  minutes and is related to flexing the foil. In the range  $3.7 \leq t \leq 7.8$  minutes, the elastic load of material takes place. The force signal changes linearly (except for a short transient period) and is accompanied by a strain change that is also linear. The value of signal  $H(t)$  is equal to zero if small fluctuations related to the measurement method are neglected.

At time  $t \approx 7.8$ , one can observe a bend in the force course and a change in the inclination angle of course  $\epsilon(t)$ , which confirms the occurrence of yield limit. It is also the beginning of the clear and constant increment of signal  $H(t)$ , which, in turn, confirms the appearance of the ferromagnetic phase (martensite  $\alpha'$ ). It is difficult to simultaneously separate in the chart the yield limit and value  $\sigma_m$  which marks the initiation of the phase transformation. The further growth

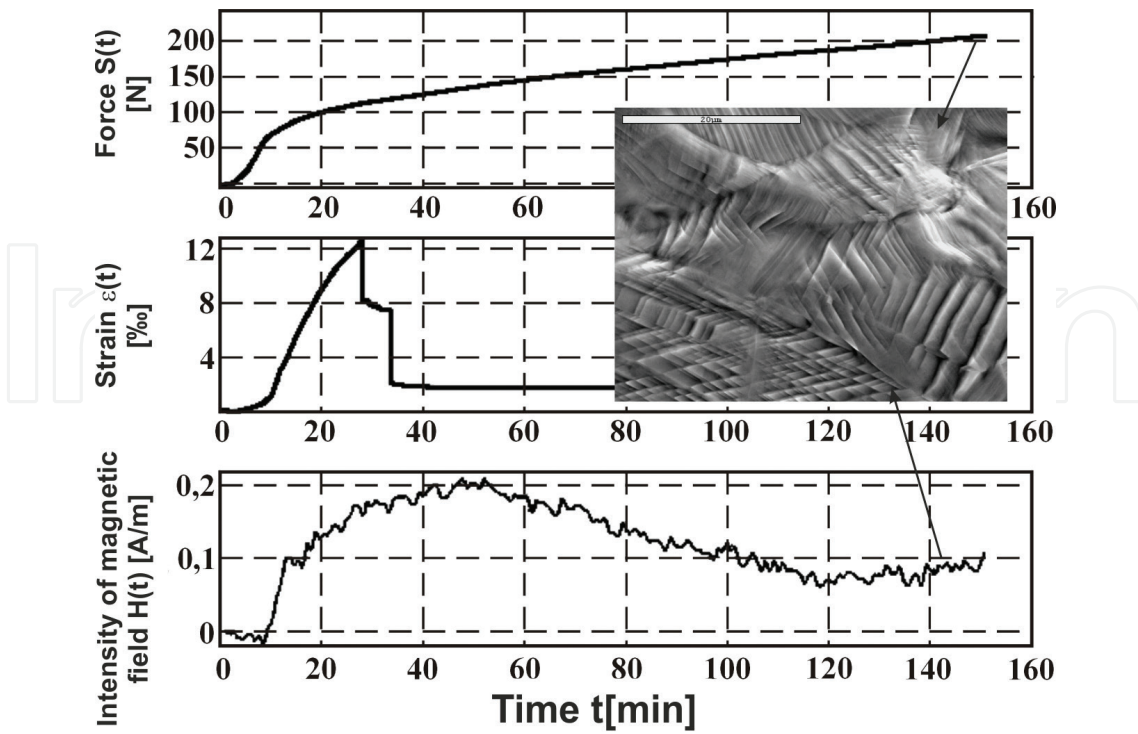


Figure 26. Characteristics  $F = f(t)$ ,  $\epsilon = f(t)$  and  $H = f(t)$ . AISI 304 steel, speed 0.035 mm/min. Additionally, the image material structure in the final part of strain (scanning microscope) [31].

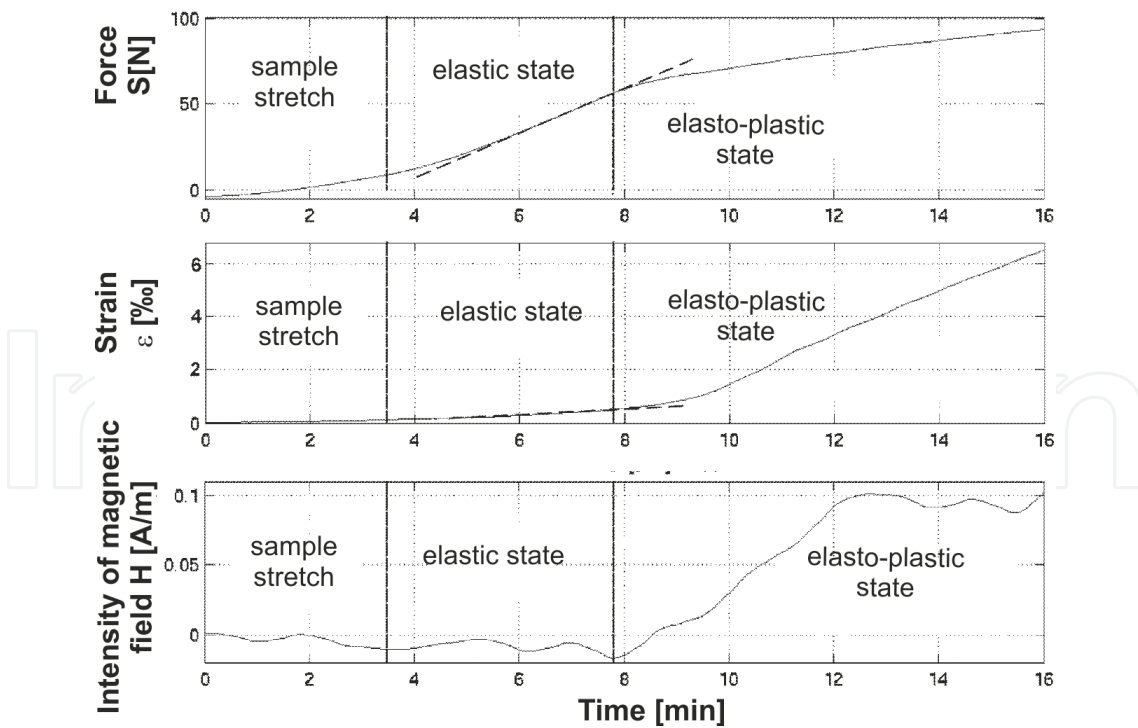


Figure 27. Characteristics  $F = f(t)$ ,  $\epsilon = f(t)$  and  $H = f(t)$ . AISI 304 steel, speed 0.035 mm/min (magnification) [31].

of strain in the plastic area results in the increment of  $H(t)$  until  $t \approx 50$  minutes and then there is a fall. This means the increment of martensite  $\alpha'$  on the one hand and on the other hand blocking the movement of domains  $n$ .

Research is currently being conducted on static strain with the simultaneous observation of changes in the structure. **Figure 26** shows a sample image of the material structure in the final phase of foil strain.

## 6. Conclusions and final remarks

The methodology of the research on the kinetics of the martensite transformation induced by plastic strain has been developed. Two cross effects (the Villari and Kelvin effects) were used for this purpose. This allowed transformations during the fatigue process to be followed and visualised on line, without the necessity to use, for example, roentgenographic or microscopic methods. The main conclusions are presented below and are divided according to the type of samples and the used cross effects:

### 1. Massive samples and magneto-mechanical effect:

- a. The measurements were conducted with the passive, contactless method using the quasi-pointwise sensors of a magnetic field (magneto-resistors). These sensors are very sensitive wideband devices (they can operate between a DC signal and a AC signal at the frequency of a few MHz).
- b. After exceeding the cyclical yield limit, the martensite transformation was initiated in a paramagnetic austenite sample, and the increment of ferromagnetic martensite  $\alpha'$  started, which was registered by a measurement head with magneto-resistors.
- c. The hydraulic pulsator and the sample form a complex magnetic system. In the measurement methodology, the assumption that the range of field changes along the sample near the zero line is linear, regardless of this obstacle, was of key significance.
- d. The notion of the zero magnetic line of the sample was introduced. Magnetic values were defined:  $H'_{0'}$  average increment of a magnetic field per unit of length of the measurement part of the sample as the magnetic measure of martensite content in the sample, and  $H''_{0'}$  martensite increment speed, respectively. Both values depend on the level of the mechanical load of the material and the number of cycles. Values  $H'_0$  and  $H''_0$  should be connected with the amount of martensite using calibration with other methods (e.g. roentgenographic or microscopic).
- e. High-resolution phase maps allowing the use of the image processing methods of such well-known techniques as machinery visioning (MV) or digital image correlation (DIC) were used in the visualisation of magnetic field changes.

### 2. Massive samples and thermo-elastic effect:

- a. The thermo-elastic effect can be used to determine the cyclic yield limit  $\sigma_{cpl}$ . For stresses  $\sigma_a < \sigma_{cpl}$ , the harmonic spectrum of temperature signal  $\Delta T(\xi)$  only includes component  $1_{sin}$ . For stresses  $\sigma_a > \sigma_{cpl}$ , higher harmonic components become visible.
- b. The moment of the initiation of the martensite transformation is manifested by the increment of the selected values of higher harmonic components (especially the second and fourth ones).

- c. The measurement method, the used apparatus, the software and the thermocouples with small thermal inertia showed that the thermomechanical effect was fully usable in the research on the fatigue process and the martensite transformation.
3. Foil samples and magneto-mechanical effect:
  - a. The martensite transformation induced by plastic strain took place in a foil 0.05 mm thick that was made of metastable austenite steel AISI 304. It was confirmed by the course of martensite signal  $H(t)$ , in which the increment was observed as a result of the occurrence of the ferromagnetic phase (martensite  $\alpha'$ ) and the recording of the Villari effect.
  - b. An original, numerically controlled test machine of 800 g was developed and made with a measurement system with mechanical and magnetic values. It proved to be very useful in the research on the phase transformation in foil samples. The device enables material strain, recording mechanical and cross signals with simultaneous observation of structural changes for the purpose of conducting the quantitative assessment of the martensite phase increment.
  - c. The martensite transformation in such thin austenite tapes is manifested by the occurrence of a very weak magnetic field (maximum 0.2 A/m), which is on the border of the maximum measurement resolution of magnetoresistors. A new more precise method of measuring a magnetic field that takes into account SQUID detectors should be considered. Additionally, it was experimentally proven that the sensitivity of magnetoresistant sensors decreases with an increase in temperature.

#### 4. Further research

Further research will focus on the calibration of the results obtained using both cross effects. Microscopic and roentgenographic methods will be employed. Such a calibration is required for each type of metastable austenite steel in which the martensite transformation induced by plastic strain takes place.

## Acknowledgements

The research was funded by project 0401/0029/17.

## Author details

Jerzy Kaleta\*, Przemysław Wiewiórski and Wojciech Wiśniewski

\*Address all correspondence to: jerzy.kaleta@pwr.edu.pl

Department of Mechanics, Materials Science and Engineering, Wrocław University of Science and Technology, Wrocław, Poland

## References

- [1] Ziętek G, Mróz Z. Thermomechanical model for austenitic steel with martensitic transformation induced by temperature and stress variation. In: Book of Abstracts of the 38th Solid Mechanics Conference, SolMech. Warsaw: Institute of Fundamental Technological Research (IPPT) of the Polish Academy of Sciences; 2012. p. 114-115
- [2] Ziętek G, Mróz Z. On the hardening rule for austenitic steels accounting for the strain induced martensitic transformation. *The International Journal of Structural Changes in Solids*. 2011;**3**(3):21-34
- [3] Ziętek G, Mróz Z. Description of cyclic hardening of material with plasticity induced martensitic transformation. In: Kotulski Z, Kowalczyk P, Sosnowski W, editors. *Selected Topics of Contemporary Solid Mechanics: Proceedings of the 36th Solid Mechanics Conference*. Warszawa: Instytut Podstawowych Problemów Techniki PAN; 2008. p. 430-431
- [4] Talonen J, Aspegren P, Hänninen H. Comparison of different methods for measuring strain induced  $\alpha$ -martensite content in austenitic steels. *Materials Science and Technology*. 2004;**20**(12):1506-1512
- [5] Nagy E, Mertinger V, Tranta F, Sólyom J. Deformation induced martensitic transformation in stainless steels. *Materials Science and Engineering: A*. 2004;**378**(1):308-313
- [6] Amitava M, De P, Bhattacharya D Sr, Srivastava P, Jiles D. Ferromagnetic properties of deformation-induced martensite transformation in AISI 304 stainless steel. *Metallurgical and Materials Transactions A*. 2004;**35**(2):599-605
- [7] Kaleta J, Zietek G. Cyclic plastic deformation-induced martensitic transformation in austenitic steels. *Advances in Fracture Research, ICF 9*. 1997;**1**:275-281
- [8] Hahnenberger F, Smaga M, Eifler D. Microstructural investigation of the fatigue behavior and phase transformation in metastable austenitic steels at ambient and lower temperatures. *International Journal of Fatigue*. 2014;**69**:36-48
- [9] Tavares S, Fruchart D, Miraglia S. A magnetic study of the reversion of martensite  $\alpha'$  in a 304 stainless steel. *Journal of Alloys and Compounds*. 2000;**307**(1):311-317
- [10] Lang M, Johnson J, Schreiber J, Dobmann G, Bassler HJ, Eifler D, Ehrlich R, Gampe U. Cyclic deformation behaviour of AISI 321 austenitic steel and its characterization by means of HTC-SQUID. *Nuclear Engineering and Design*. 2000;**198**(1):185-191
- [11] Shin HC, Ha TK, Chang YW. Kinetics of deformation induced martensitic transformation in a 304 stainless steel. *Scripta Materialia*. 2001;**45**(7):823-829
- [12] Kaleta J, Lewandowski D, Wiśniewski W. Kinematics of cross effects in cyclic load induced martensitic transformation in massive specimens. In: *Scientific Letters of Kielce University of Technology, Kielce*. Vol. 73. 2001. p. 391-400

- [13] Kaleta J, Tumański S, Żebracki J. Magneto-resistors as a tool for investigation of mechanical properties of ferromagnetic materials. *Journal of Magnetism and Magnetic Materials*. 1996;**160**:165-166
- [14] Kaleta J, Susz S. Magnetovision system for examination of biaxial stress state under cyclic load. In: *Experimental Mechanics of Solids - 17th Symposium*, Jachranka, Poland, 1996. p. 290-295 (in Polish)
- [15] Thomson W. On the dynamical theory of heat. *Transactions of the Royal Society of Edinburgh*. 1853;**20**:261-283
- [16] Kaleta J, Moczko P, Wiśniewski W. Harmonic analysis of temperature signal in thermo-elastic effect for austenite under cyclic load. In: *Experimental Mechanics of Solids - 19th Symposium*, Jachranka, Poland, 1996. Vol. 2000. p. 296-301 (in Polish)
- [17] Kaleta J, Ziętek G. Cyclic plastic deformation-induced martensitic transformation in austenitic steels. In: *Proceedings of 9th International Conference on Fracture ICF-9*, Pergamon, Sydney. Vol. 1. April 1-5, 1997. p. 275-281
- [18] Kaleta J, Wiśniewski W, Wiewiórski PK. Magnetic method of testing martensitic transformation induced by plastic deformation in solid specimens of AISI 304. In: *Symposium on Fatigue and Mechanics of Materials and Structure*, Bydgoszcz-Pieczyska. 2008. p. 139-145 (in Polish)
- [19] Kaleta J, Wiewiórski PK, Wiśniewski W. Methods of testing martensitic transformation induced by plastic deformation in solid specimens. In: *Experimental Mechanics of Solids - 23th Symposium*, Jachranka, Poland, 2008 (in Polish)
- [20] Kaleta J, Żebracki J. Application of the Villari effect in fatigue examination of nickel. *Fatigue and Fracture of Engineering Materials and Structures*. 1996;**19**(12):1435-1443
- [21] Kaleta J, Wiewiórski P. Magnetic field distribution detecting and computing methods for experimental mechanics. *Engineering Transactions*. 2010;**58**(3/4):97-118
- [22] Kaleta J, Wiewiórski P. Magnetovisual method for monitoring thermal demagnetization of permanent magnets used in magnetostrictive actuators. *Journal of Rare Earths*. 2014;**32**(3):236-241
- [23] Tumański S, Stabrowski M. Magnetovision system, new method of investigating steel sheets. *Journal of Magnetism and Magnetic Materials*. 1996;**160**:165-166
- [24] Philips Semiconductor "Magneto-resistive Sensors for Magnetic Field Measurement", Application Manual SC17 Rev. 2, Sep 6, 2000
- [25] Gasparics A. Electromagnetic Nondestructive Material Evaluation Based on Fluxset Sensor, [PHD thesis]. Budapest University of Technology and Economics; 2005
- [26] Yang CH, Tsai MC. Measurement of magnetic fields by B-spline method. *Journal of Magnetism and Magnetic Materials*. 2006;**304**:460-463

- [27] Tan S, Ma YP, Thomas IM, Wikswo JP Jr. High resolution SQUID imaging of current and magnetisation distributions. *IEEE Transactions on Applied Superconductivity*. 1993;**3**(1):1945-1948
- [28] Lo CCH, Paulsen JA, Jiles DC. A magnetic imaging system for evaluation of material conditions using magnetoresistive devices. *IEEE Transactions on Magnetics*. 2003;**39**(5):3453-3455
- [29] Infante F, Perdu P, Lewis D. Magnetic microscopy for ground plane current detection: A fast and reliable technique for current leakage localization by means of magnetic simulations. *Microelectronics Reliability*. 2010;**50**:1700-1705
- [30] Dodd RK. A new approach to the visualization of tensor fields. *Graphical Models and Image Processing*. 1998;**60**:286-303
- [31] Dubov A, Kolokolnikov S. The metal magnetic memory method application for online monitoring of damage development in steel pipes and welded joints specimens. *Weld World*. 2013;**57**:s123-s136
- [32] Fassa B, Kaleta J, Wiewiórski PK. Plastic strain induced martensitic transformation in foils with metastable austenite. In: *Scientific Letters of Kielce University of Technology* 2001. p. 343-350 (in Polish)
- [33] Fassa B, Kaleta J. Identification of kinetics martensitic transformation induced by plastic strain in austenitic foils. In: *Scientific Letters of Kielce University of Technology*. Vol. 4, 2007. p. 27-29 (in Polish)

